Ore Geology Reviews 72 (2016) 1143–1162

Contents lists available at ScienceDirect

Ore Geology Reviews

journal homepage: www.elsevier.com/locate/oregeorev

Evolution of Montviel alkaline–carbonatite complex by coupled fractional crystallization, fluid mixing and metasomatism — part I: Petrography and geochemistry of metasomatic aegirine–augite and biotite: Implications for REE–Nb mineralization

Olivier Nadeau [a,*], R. Stevenson [b], M. Jébrak [b]

[a] Department of Earth Sciences, University of Ottawa, Ottawa, K1N 6N5, Canada
[b] Département des Sciences de la Terre et de l'Atmosphère, Université du Québec à Montréal, Montréal, H2X 3Y7, Canada

ARTICLE INFO

Article history:
Received 31 July 2015
Received in revised form 17 September 2015
Accepted 21 September 2015
Available online 25 September 2015

Keywords:
Alkaline and carbonatite magmas
Assimilation, fractional crystallization and metasomatism
Magmatic–hydrothermal evolution
Mantle pulses
Sm–Nd isotopes

ABSTRACT

Magmatic volatiles are critically important in the petrogenesis of igneous rocks but their inherent transience hampers the identification of their role in magmatic and mineralization processes. We present evidence that magmatic volatiles played a critical role in the formation of the 1894 Ma Paleoproterozoic Montviel alkaline–carbonatite complex, Canada, and the related carbonatite-hosted REE–Nb deposit. Field and drill core relationships indicate that lithological units of the complex were emplaced in the following order: clinopyroxenites, melteigites, ijolites, melanosyenites, leucosyenites, granites, lamprophyric silicocarbonatites, rare magnesiocarbonatites, calciocarbonatites, ferrocarbonatites, late mixed carbonatites, kimberlitic silicocarbonatites and polygenic breccias. Magmatic minerals within these units were systematically metasomatized. In undersaturated silicate rocks, augite recrystallized to aegirine–augite and aegirine, plagioclase recrystallized to albite, and nepheline recrystallized with analcime, cancrinite and albite. Primary biotite was replaced by secondary, REE-rich metasomatic biotite, particularly along fractures and alteration pockets. In carbonatites, liquidus phases consisted of calcite and dolomite and were recrystallized to ferroan dolomite, ankerite, siderite, barytocalcite, witherite and strontianite, which are intimately related to the REE-bearing carbonates and fluorocarbonates. Biotite is common to all lithologies, ranges in REE concentrations from 1.5 to 230 ppm and yielded subsolidus crystallization temperatures ranging from 770 °C to 370 °C. Sm–Nd isotope analyses from biotite and aegirine–augite yield a range of ε_{Nd} values (+3.4 to −3.0) that suggests mixing of fluids from three sources during the crystallization of the Montviel magmas. The clinopyroxenites to melteigite, ijolites and melanosyenites crystallized augite and biotite with initial ε_{Nd} value ≥ 3.4 and these minerals were metasomatized by a 1st fluid, lowering their ε_{Nd} to values comprised between 0.8 and 3.4. Silicocarbonatites and carbonatites subsequently crystallized aegirine–augite and biotite with initial ε_{Nd} value ≥2.6 and a 2nd fluid metasomatized the minerals to lower ε values. Both the 1st and the 2nd fluids eventually mixed with a 3rd recrystallizing aegirine–augite and biotite and lower their εNd values down to −3.0. The results presented herein suggest that the mantle magmas evolved through 4 distinct mantle pulses by fractional crystallization, mixing of depleted mantle fluids with crustal fluids, and metasomatism. Some of the silicate rocks also show evidence of assimilation of wall rock as part of their petrogenetic evolution. During the last stages of its evolution in carbonatites, the fluid source transited from the depleted mantle to the crust and we speculate that this resulted in a violent explosive eruption creating the diatreme-shaped, HREE-rich polygenic breccia.

Contents

* Corresponding author.
E-mail address: onadeau@uottawa.ca (O. Nadeau).

http://dx.doi.org/10.1016/j.oregeorev.2015.09.022
0169-1368/

1. Introduction

Magmatic volatiles are critically important in the petrogenesis of igneous rocks but their inherent transience hampers the identification of their role in magmatic and mineralization processes (e.g., Bowen, 1928; Hamilton et al., 1964; Hedenquist and Lowenstern, 1994; deMoor et al., 2013; Black et al., 2014; Plail et al., 2014). The role of magmatic volatiles in porphyry copper systems, for example, is relatively well understood (e.g., Sillitoe, 1973, 2010), but understanding the behavior of volatiles and metasomatic fluids in mantle and crustal magmatic–hydrothermal systems remains a work in progress.

Metasomatism is widely used to describe the chemical alteration of solid rocks and minerals by external fluids, but the definition of metasomatism (e.g., Lindgren, 1933; Ramberg, 1952; Best and Christiansen, 2001; Pirajno, 2013) does not exclude the possibility that partially crystallized magmas may start being metasomatized by their own fluids: autometasomatism is a special case of metasomatism whereby the metasomatic agent is sourced from the same magmas that are being metasomatized (e.g., Elsdon, 1982). In a magmatic–hydrothermal context this necessitate that (1) the magmatic volatile phase be exsolved from the melt but stay in the magma as it crystallizes, and (2) either the rock or the fluid change its chemical composition so they lose their thermodynamic equilibrium. The loss of thermodynamic equilibrium between the magmatic fluid and the solidifying rocks can be achieved, for example by fractional crystallization of the magma and mixing of the magmatic volatile phase with external fluids.

Alkali metasomatism by K and Na has been documented in several types of magmatic–hydrothermal systems such as in the high temperature K alteration of porphyry deposits (e.g., Seedorff et al., 2005) and the high temperature Na alteration common to IOCG-type and affiliated deposits (e.g., Corriveau, 2007; Richards, 2014). Potassium metasomatism (or potassic alteration) is usually associated with minerals such as microcline (adularia), biotite and sericite, whereas Na metasomatism recrystallizes minerals such as albite, riebeckite, aegirine–augite and aegirine. Different rocks show distinct kinds of metasomatism as K-Na metasomatism is more common to ijolites whereas carbonatites are usually associated with intense K metasomatism (Pirajno, 2013), and both processes are often referred to as fenitization. It has been shown that Fe was introduced hydrothermally in large-scale mineralized systems such as that of Olympic Dam district, Australia (Bastrakov et al., 2007) and Bayan Obo, China (Smith et al., 2015), recrystallizing minerals such as magnetite, hematite, Fe-bearing carbonates, pyrite, and Fe silicates such as biotite and other Fe-bearing silicates. Metasomatism has been documented in different tectonic settings such as subduction zones (e.g., Bebout, 2013), collisional orogeny (e.g., Touret and Nijland, 2013), rifts (e.g., Dupuy et al., 1991) and in the mantle (e.g., O'Reilly and Griffin, 2013).

The Montviel alkaline complex, Canada, represents and ideal setting to study the role of metasomatism in the evolution of magmatic–hydrothermal systems because: (1) of the presence of diverse lithologies, (2) each of the lithologies was metasomatized; and (3) the alkaline complex was extensively drilled for core samples which were readily available for this study. This study presents the petrography of the lithologies and establishes a paragenetic mineral sequence based on field work and drill core relations (Goutier, 2006; Nadeau et al., 2015). The surface geology, the major element composition of bulk rocks, biotites, clinopyroxenes and tectosilicates, the rare earth element (REE) concentration in biotite and the Sm–Nd isotopic ratios of biotite and aegirine–augite are reported

and discussed with emphasis on the role of metasomatism in the petrogenesis of the rocks and on the source of the fluids. The trace element and Sm–Nd isotopic composition of bulk rocks are presented in a companion paper titled: "Evolution of Montviel Alkaline–Carbonatite Complex by Coupled Fractional Crystallization, Fluid Mixing and Metasomatism — Part II: Trace Element and Sm–Nd Isotope Geochemistry of Metasomatic Rocks; Implications for REE–Nb mineralizations".

2. Tectonic and geologic context

The Subprovinces of the Superior Craton of Laurentia were assembled into a single Archean craton by the end of the Archean (Kerrich and Cassidy, 1994; Mueller et al., 1996). The Proterozoic was characterized by the collision of numerous cratons around the world between 2000 Ma and 1750 Ma (Condie et al., 2015). On the east side of the Superior, eastward subduction was initiated at 2170 Ma and resulted in the formation of the New Quebec Orogen between 1870 and 1815 Ma. Similarly, north of the Superior, subduction was onset at 1980 Ma, resulting in the Trans-Hudson orogenesis from 1850 to 1800 Ma (Condie et al., 2015). Although no major tectonic activity is reported at these times within the Superior, a number of alkaline intrusions were emplaced within the Superior Craton such as the 1894 Ma Montviel alkaline–carbonatite complex in the Abitibi Subprovince (David et al., 2006), the 1907 Ma Cargill pyroxenite–carbonatite complex (Sage, 1988) and the 1872 Ma Borden silicocarbonatite–carbonatite complex (Bell et al., 1987) in the Kapuskasing Subprovince. The origin of Montviel, Cargill and Borden alkaline–carbonatite complexes is unclear but is probably related to the subductions, collisions and post-collision relaxations occurring on the outskirts of the craton and the related readjustments along major fault zones. Montviel is located within a fault network that extends for over 235 km between Matagami and Chibougamau and less than 10 km away from major regional thrusts of the greenstone belt (Goutier, 2006).

The Paleoproterozoic Montviel alkaline–carbonatite complex intruded foliated Archean tonalites in the northeastern part of the Abitibi Subprovince at 1894 ± 4 Ma, based on U–Pb on zircons from the ijolite units (David et al., 2006). A chronological sequence of the lithological units was established based on field and drill core cross-cutting relationships (Goutier, 2006; Nadeau et al., 2015). The alkaline system consisted of injections of clinopyroxenites, melteigites, ijolites, melanosyenites, leucosyenites, granites, lamprophyric silicocarbonatites, rare magnesiocarbonatites, calciocarbonatites, ferrocarbonatites, late mixed carbonatites, kimberlitic silicocarbonatites and polygenic breccias (Fig. 1). The intrusion is neither deformed nor metamorphosed. Based on underground mapping, the carbonatite is cut by a main NNW–SSE fault and a

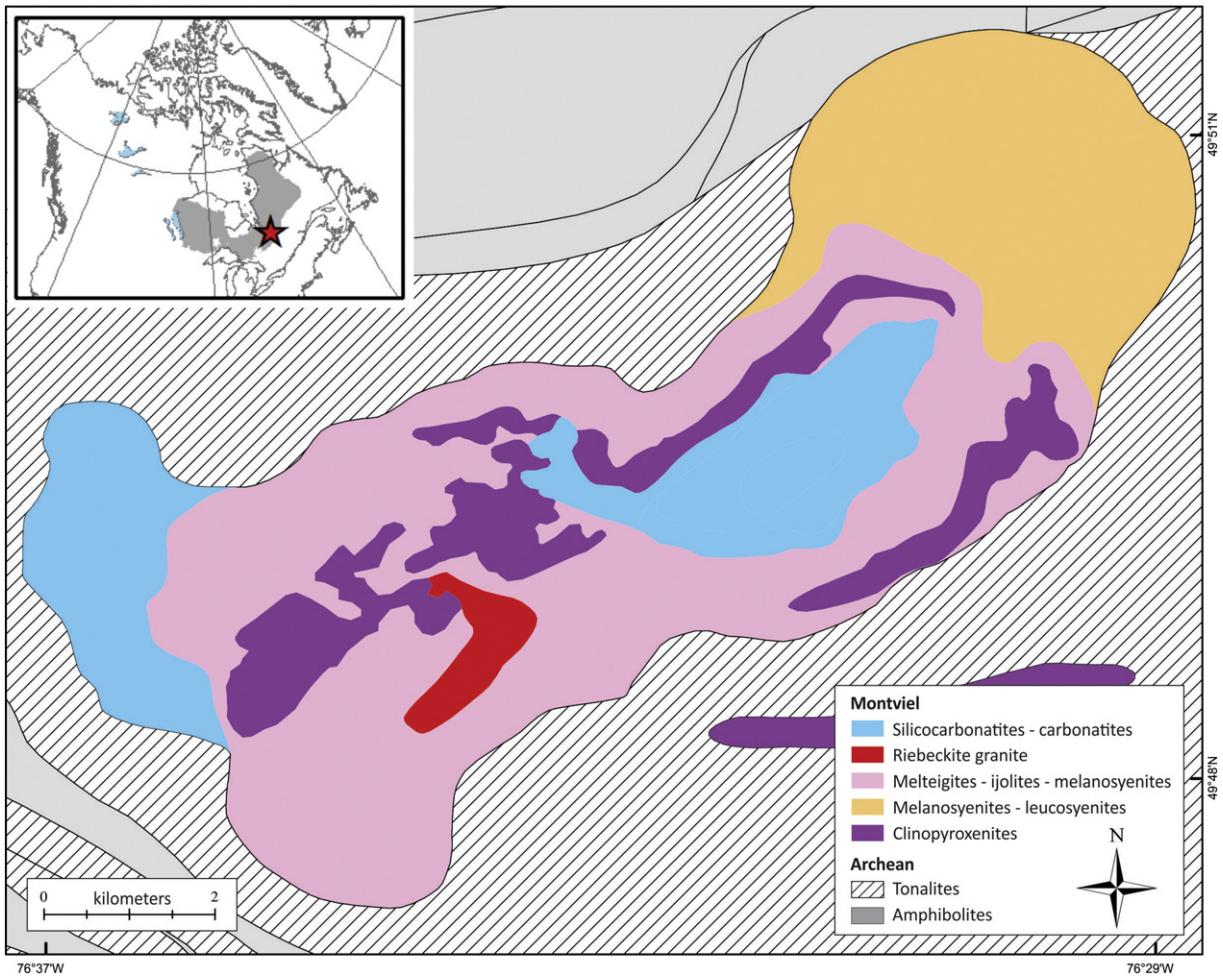

Fig. 1. Surface geology of Montviel alkaline complex. Inset map shows the location of Montviel alkaline complex within the Archean Superior craton (in gray) and North America. Modified after Goutier (2006).

series of second order NE–SW faults, although the faults appear to have allowed very little displacement (Nadeau et al., 2015). The carbonatite, and especially the ferrocarbonatite and the polygenic breccia host a REE–Nb deposit, which consist of REE carbonates and fluorocarbonates associated with zones of hydrothermal Ba–Sr–P–F alteration (Nadeau et al., 2015).

3. Analytical methods

3.1. Petrography

Polished sections were prepared and observed using a Leica DMLP petrographic microscope equipped with Leica DFC450 digital camera

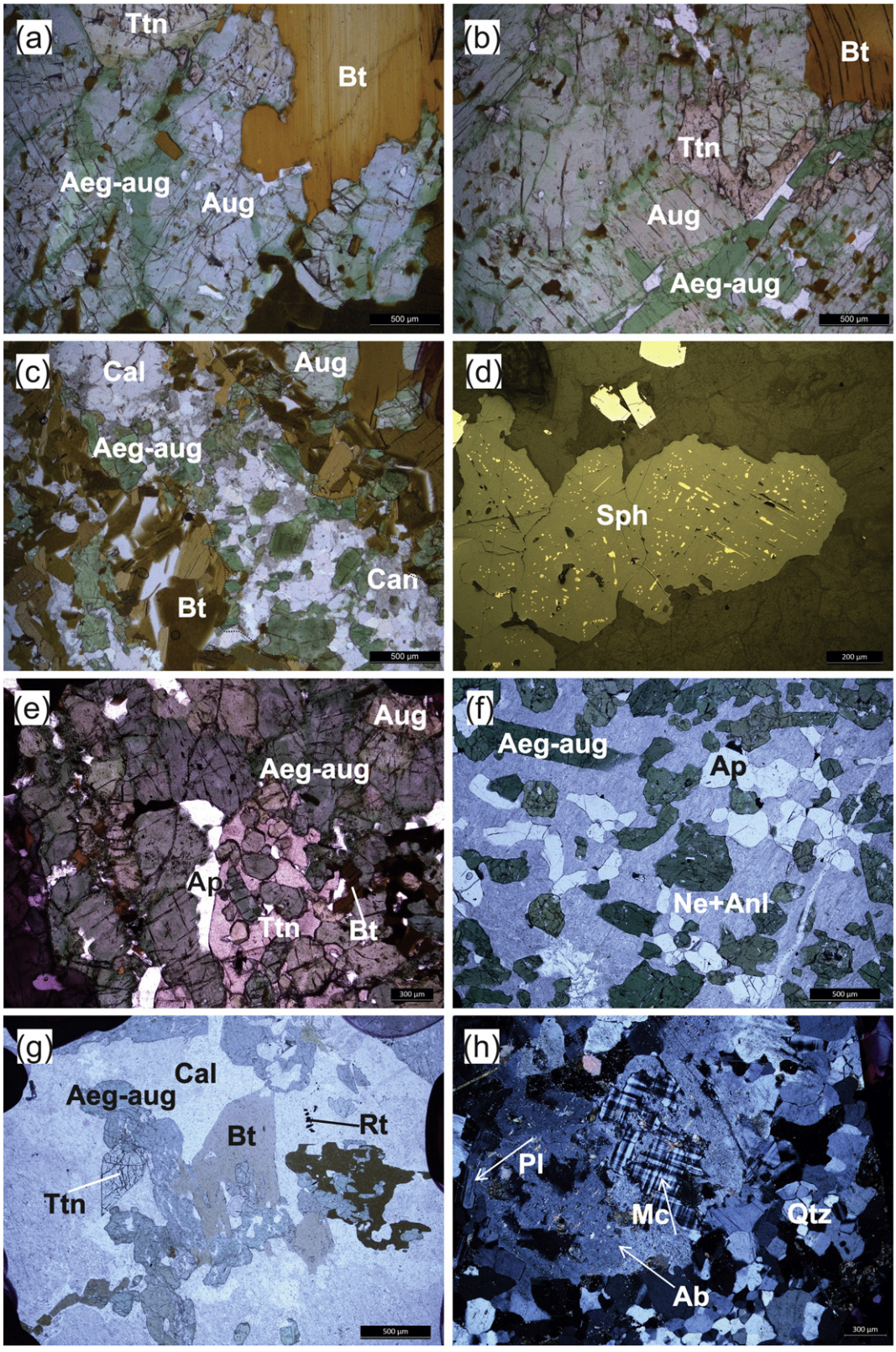

and using a Hitachi TM3000 tabletop scanning electron microscope (SEM) equipped with a Bruker Quantax 70 energy dispersive X-ray spectrometer (EDS).

3.2. X-ray diffraction

Powdered bulk rock samples were scanned using a Siemens D500 X-ray diffractometer equipped with a Co tube and a Si detector at UQAM. X-ray diffraction spectra were identified using Eva software version 1.3.

3.3. Electron microprobe

Biotite, clinopyroxene, amphibole and a variety of tectosilicates were analyzed for a selection of major to minor elements using a JEOL JXA-8900 L electron microprobe, with a 15 kV and 20 nA beam, in the Geochemical Laboratories, McGill University. The beam diameter was 10 μm for biotite, pyroxene and amphiboles and 50 μm for tectosilicates. For biotite, counting times for most elements were 20 s and detection limits varied between about 200 and 500 ppm. A counting time of 100 s was used for F, returning detection limits of about 700 ppm, and 200 s for Cl and S, returning detection limits of 85 and 140 ppm, respectively. For pyroxene and amphibole, counting times were 20 s for all elements, returning limits of detection of about 200–500 ppm, except for F which had a limit of detection of 1200–1500 ppm. For tectosilicates counting times were also of 20 s, resulting in detections limits of about 200–500 for most elements except F (1500–2000 ppm) and Ba (700–1000 ppm). The instrument was calibrated using a set of commercial and in-house standards and relative standard deviations (1σ) were generally less than 1% (e.g., CaO = 20 ± 0.2 wt.%).

3.4. Laser ablation ICP-MS

Attempts to analyze the same biotite crystals for REE concentrations using a laser ablation ICPMS system were made at the Geotop, UQAM. The system consists of a Photon-machines Analyte.193 G2 Pulse Excimer laser and a Nu Instrument Attom, high resolution, sector field ICPMS. A NBS610 glass standard was used as external standard and the concentrations of REE were quantified using Ti obtained from the electron microprobe as the internal standard.

3.5. Thermal ionization mass spectrometry (TIMS)

Sm–Nd isotopes were analyzed at Geotop, UQAM. Sample weighing and chemistry were performed in a class 100 (ISO5) clean room. Powdered samples were weighed (about 0.1 g) and a ^{149}Sm–^{150}Nd spike was added to determine Sm and Nd concentrations. The samples were sequentially dissolved and dried in 29 N HF, 29 N HF + 15 N HNO_3, Aqua Regia and 6 N HCl acids. The Sm and Nd fractions were then purified by cation exchange chromatography following the procedure of Roulleau and Stevenson (2013). The Sm and Nd isotopes samples were measured in static collection mode via a double Re filament assembly on a Thermo Scientific Triton Plus thermal ionization mass spectrometer (TIMS). Neodymium was monitored using a JNd1 standard having a value of $^{143}Nd/^{144}Nd = 0.51209 \pm 0.00005$ and 2σ errors were 0.000009 in average (n = 19). Typical combined procedure blanks for Nd and Sm were <150 pg.

4. Petrography

4.1. Clinopyroxenites

In the field and in drill cores, clinopyroxenites, melteigites, ijolites and melanosyenites are observed as dykes, pods and sills that cross-cut each other. For example, clinopyroxenite commonly hosts dykes, pods and sills of ijolite and melanosyenite whereas ijolites and melanosyenites commonly host dykes, pods and sills of clinopyroxenite. The geological map in Fig. 1 thus, represents a simplified geology and is based on the work of Goutier (2006). Clinopyroxenites consist of coarse augite, titanite and biotite with pyrrhotite, chalcopyrite, sphalerite and ilmenite. Augite is systematically metasomatized to aegirine–augite along fractures and grain boundaries and is also sometimes to biotite (Figs. 2a–c, 3b). Accessory minerals include zircon, apatite, feldspathoids such as nepheline and sodalite, analcime (a zeolite), cancrinite (a pseudo-zeolite), and other tectosilicates such as albite–celsian (a Na–Ba–feldspar) (Figs. 2e–g and 3a, c, d, e). In clinopyroxenite, all tectosilicates (feldspathoids, zeolites, pseudo-zeolites and albite) display secondary alteration or recrystallization textures (Fig. 3b, c, e). Calcite, dolomite and ankerite are present.

4.2. Melteigites and ijolites

The melteigites and ijolites are found in association with clinopyroxenites and melanosyenites and are always metasomatized. Melteigites consist of coarse augite altered to aegirine–augite and aegirine, along with significant amounts of coarse biotite, titanite and fluorapatite (Fig. 3b, d). Abundant microscopic nepheline, sodalite, cancrinite and analcime appear to be secondary (Figs. 2f, 3b, e). The ijolites are very similar to melteigites but contain less clinopyroxene and more nepheline and analcime.

4.3. Syenites and granites

The syenites are commonly associated with melteigites–ijolites and clinopyroxenites and range in composition from K-feldspar clinopyroxenites to quartz leucosyenites. They resemble ijolites but contain greater amounts of microcline and albite and less nepheline, cancrinite and analcime. The melanosyenites consist of ferropotassic magnesiohastingsite, riebeckite, aegirine–augite and microcline. Aegirine–augite and albite are secondary. The leucosyenites (Fig. 2h) are the only quartz-saturated rocks of the alkaline complex, along with the riebeckite granite described below, and occur only in the NE end of the alkaline complex.

Fig. 2. Photomicrographs of silicate rocks showing mineral and texture relations. Photographs are in transmitted, single-polarized light unless otherwise stated. (a–b) Clinopyroxenite showing magmatic augite (Aug) with zones of metasomatic aegirine–augite (Aeg–aug) and biotite (Bt) along grain boundaries and fractures. Coarser biotite also occurs in decussate texture with augite. Titanite (Ttn) and augite display inclusions of apatite, ilmenite, chalcopyrite, silicate and carbonatite melt (Sample MV12.IJ02). (c) Biotite clinopyroxenite with augite, aegirine–augite and biotite, cut by dyklets of calcite, aegirine–augite and cancrinite (Can) (Sample MV12.IJ02). (d) Reflected light photomicrograph of sphalerite (Sph) with Cu-rich sulfide melt inclusions (intermediate solid solution) aligned along crystallographic growth planes (chalcopyrite disease), in the carbonatite part of a glimmerite breccia (Sample LP12.UMBX01). (e) Clinopyroxenite showing more or less metasomatized augite, titanite, fluorapatite and biotite. Biotite appears to be hydrothermal as it occurs along grain boundaries and fracture zones. The alteration also includes Ca-rich strontianite and nepheline (not shown) (Sample MV12.UM04). (f) Ijolite consisting of euhedral but metasomatized aegirine–augite and fluorapatite in a matrix of intermixed nepheline (Ne) and analcime (Anl). The BSE view of the nepheline–analcime mix shows skeletal nepheline in a matrix of analcime (Fig. 3e). Other areas of the same polished section also show euhedral analcime (Sample MV12.SY02). (g) Same ijolite as in panel f, showing aegirine–augite, biotite, calcite, titanite and rutile (Rt). The small dark crystals in the upper-right are rutile with amounts of Nb detectable under the EDS. The titanite crystal has concentrations of Zr detectable under the EDS and hosts inclusions of calcite, zircon and aegirine–augite (Sample MV12.SY02). (h) Crossed polar view of the quartz-saturated leucosyenite showing euhedral plagioclase (Pl) and quartz (Qtz) with metasomatic microcline (Mi) with tartan twin, and albite (Ab) (Sample MV12.SY04).

The riebeckite granites outcrop only in the southern part of the intrusion and are mapped as a single unit (Fig. 1). They resemble the leucosyenites but contain significantly more quartz and plagioclase, and relatively less microcline. Biotite and riebeckite are present in minor amounts. Hydrothermal alteration has altered plagioclase to albite and produced riebeckite from an unidentified ferromagnesian mineral.

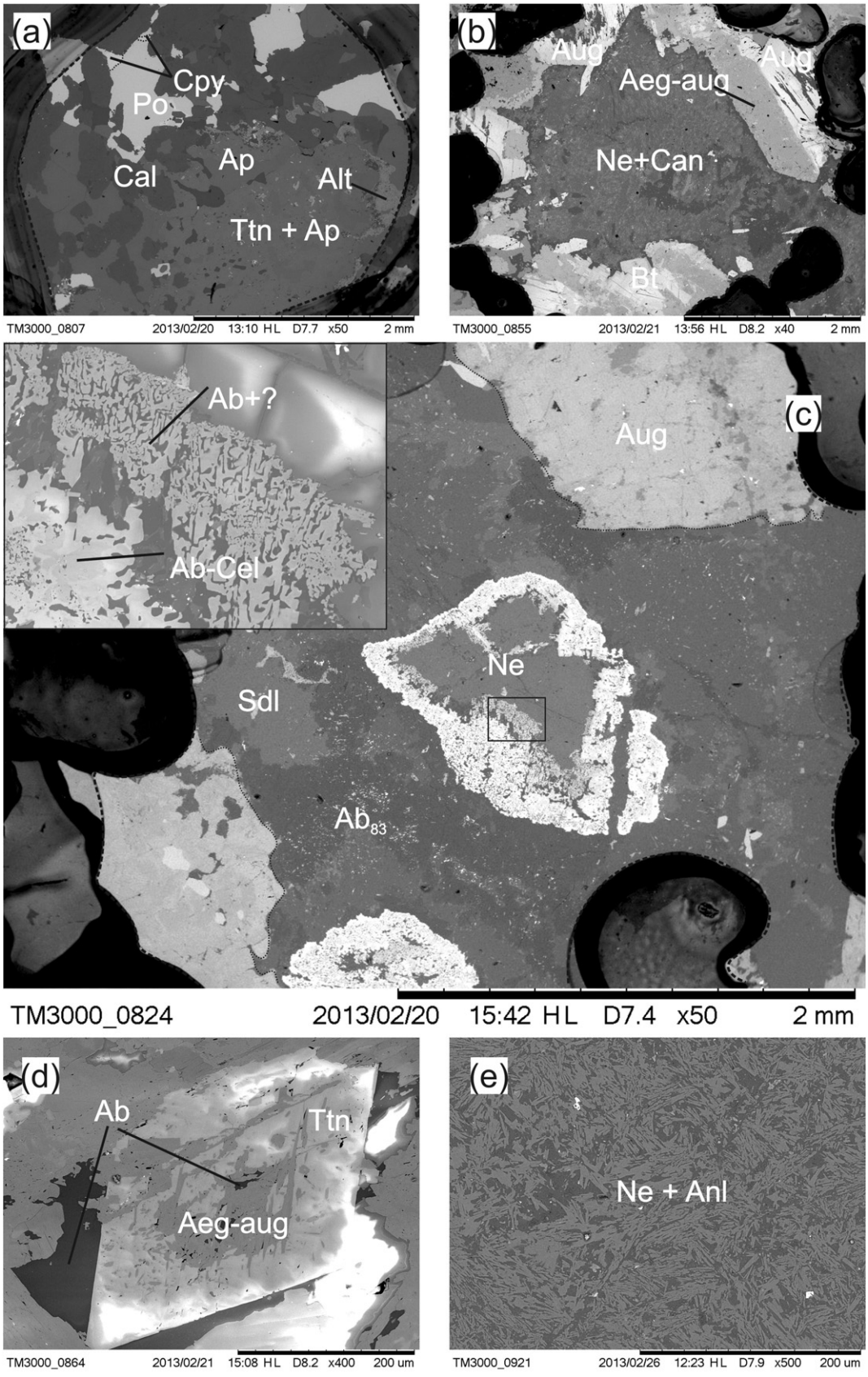

4.4. Silicocarbonatites

Silicocarbonatites at Montviel have compositions intermediate between ultramafic undersaturated silicate rocks (clinopyroxenites, melteigites, ijolites and melanosyenites) and carbonatites, and contain 10–50% magmatic carbonate minerals. Silicocarbonatites are subdivided into lamprophyric- (Figs. 4b and 5a, b), glimmerite breccias (Figs. 4a, d, e, and 5d) and (3) kimberlitic silicocarbonatites (Figs. 4c and 5c). The terms 'lamprophyric' and 'kimberlitic' are introduced to enable distinction of the two types of silicocarbonatites and because the silicocarbonatites have visual similitude with ultramafic lamprophyres and kimberlites. Lamprophyric silicocarbonatites are most common and consist of kinked or folded booklets of biotite (Figs. 4b and 5a) and pseudomorphs of olivine in a matrix of dolomite, ankerite, calcite and pyrite. Glimmerite breccias consist of decussate-texture glimmerites brecciated by dyklets of carbonates (Fig. 4a). Kimberlitic silicocarbonatites are found mainly as a 50 m wide dyke cross-cutting through all silicate rocks and carbonatites and consist of breccias made of altered fragments and xenocrysts of carbonates and ferromagnesian rocks in a hydrothermally-altered matrix of biotite and other minerals. They texturally and visually resemble kimberlites but with higher amounts of carbonates, lesser amounts of K-bearing minerals and no fresh olivine.

4.5. Carbonatites

The magnesiocarbonatites are rare and occur as pods and lenses intermixed with other types of carbonatites and silicocarbonatites, and are dominated by dolomite of magmatic origin. Carbonates of Ba–Ca–Mg (Ca-bearing norsethite or Ba-bearing dolomite?), barytocalcite, strontianite, fluorite, REE carbonates and fluorocarbonates and albite are hydrothermal and present in major concentrations (Fig. 6a).

Calciocarbonatites are dominated by calcite and range from barren and unaltered calcite carbonatite to REE-bearing, hydrothermally altered calciocarbonatites. Calciocarbonatites contain major amounts of primary calcite and dolomite which are cut by veinlets of ankerite, strontianite, witherite and barytocalcite and contain minor to trace concentrations of aegirine–augite, biotite, fluorapatite (Fig. 7a), barite and REE carbonates and fluorocarbonates.

Ferrocarbonatites are the most abundant type of carbonatites, cross-cut the calciocarbonatites and are strongly and pervasively hydrothermally altered. They are dominated by hydrothermal or metasomatic ankerite and Fe-dolomite, siderite, barytocalcite, strontianite, witherite, fluorite, fluorapatite and minor to trace amounts of biotite, aegirine, arfvedsonite, barite, REE carbonate and fluorocarbonate, monazite-(Ce), xenotime-(Y), loparite (REE perovskite), sphalerite and galena (Figs. 6c and 7c–f).

The hydrothermally altered ferrocarbonatites are cross-cut by injections of mixed silicocarbonatites, calciocarbonatites and ferrocarbonatites gathered under the term of 'mixed carbonatites'. These mixed carbonatites were also hydrothermally altered to various degrees with alteration products similar to those described above. Their existence clearly demonstrates that carbonatites were injected repeatedly and that episodes of magmatism both preceded and followed episodes of hydrothermal alteration. The mixed carbonatites show zones of alterations with REE fluorocarbonates (qaqarssukite, carbocernaite), barite, biotite and chlorite in calcite (Fig. 7b, g).

4.6. Polygenic breccias

The polygenic breccias consist of clasts and xenocrysts of silicocarbonatites and carbonatites in a pervasively altered matrix of dolomite, calcite, ankerite, strontianite, barytocalcite, fluorapatite, biotite, aegirine–augite, and ferropotassic magnesio-hastingsite. Three-dimensional modeling of the breccia fragments suggests that the shapes are a hybrid between dykes and a diatreme (Nadeau et al., 2013) and Nadeau et al. (2015) proposed that the breccia unit formed as a result of high-energy fragmentation with significant displacement based on modeling of the distribution and size of the fragments (Jébrak, 1997) and three dimensional modeling of the deposit based on drill core data. This explosion was the last event of the emplacement of the Montviel alkaline complex (Figs. 6e and 7h).

5. Mineral paragenesis

A mineral paragenesis (Fig. 8) was established based on relative chronology of petrological observation in the field and drill cores (Goutier, 2006; Nadeau et al., 2015). The lithological units are ordered chronologically as mentioned above. A large dyke of kimberlitic silicocarbonatite cuts through all lithologies except the polygenic breccia and is thus positioned near the end immediately before the polygenic breccia. Magnesiocarbonatite is very rare (1 occurrence) but intimately associated with calciocarbonatite, so it was arbitrarily placed before calciocarbonatite.

Olivine was only observed in three of the lithologies: as pseudomorphs in clinopyroxenites and kimberlitic silicocarbonatites and as a minor unaltered occurrence in the polygenic breccias. Augite is only found in clinopyroxenites and melteigites whereas aegirine–augite was the most common clinopyroxene in all ultramafic and mafic silica-deficient rocks. Aegirine was observed in ferrocarbonatites. Alkaline amphiboles such as ferropotassic magnesio-hastingsite, riebeckite and arfvedsonite were identified in melanosyenites, ferrocarbonatites and kimberlitic silicocarbonatites, respectively. It is noteworthy that biotite and fluorapatite were present throughout the evolution of the complex.

Nepheline, sodalite, cancrinite and analcime were observed in clinopyroxenites, melteigites and ijolites (Fig. 8). Cancrinite was also seen in lamprophyric silicocarbonatites. Microcline and plagioclase were identified in melanosyenites and leucosyenites whereas quartz was found only in leucosyenites and granites. In the silicate rocks, feldspathoids were found to occur in the early units, microcline and plagioclase crystallized in the intermediate units and quartz crystallized in the last silicate rocks. Metasomatic and/or hydrothermal albite was observed in all silicate rocks. Following the silicate magmas, the alkaline complex was injected with silicocarbonatite and carbonatite magmas where no tectosilicates was found except for albite in some silicocarbonatites and magnesiocarbonatites samples.

Except for ankerite which was hydrothermal, calcite and dolomite were the only carbonates to crystallize in the primitive silicate rocks. In contrast, strontianite, siderite, barytocalcite and witherite were always hydrothermal and found solely in carbonatites. Primary sulfides consisted on pyrrhotite, chalcopyrite, sphalerite and galena. Mostpyrite is secondary and appears to have resulted from low temperature recrystallization, except for some primary pyrite which formed during the last

Fig. 3. Backscatter electron image of silicate rocks showing mineral and texture relations.(a) Clinopyroxenite consisting of augite (not shown) accompanied by fluorapatite, calcite, titanite and fluoroapatite (Ap). The presence of pyrrhotite (Po) and chalcopyrite (Cpy) (formerly monosulfide and intermediate solid solutions) testifies of the relatively reducing conditions and the high activity of sulfur in the magma. Titanite is poikilitic with inclusions of carbonatite melt and fluorapatite. A zone of alteration (Alt) consists of a mix of unidentified O–Ca–Fe–Ti–Zr–Nb (brannerite? polymignite?) and Zr–O (baddeleyite?) phases and fluorapatite (Sample MV12.UM01). (b) Melteigite made mostly of aegirine–augite (Aeg–aug) and augite (Aug), here showing the secondary nature of the subordinate nepheline (Ne) and cancrinite (Can) (sample MV12.IJ01). (c) Zone of metasomatic replacement in clinopyroxenite, recrystallizing an assemblage of nepheline, sodalite (Sdl) and albite–celsian (inset) (Sample MV12.UM04). (d) Aegirinization and albitization of titanite in melteigite. Titanium was mobile (sample MV12.IJ01). (e) Skeletal nepheline and analcime in the same ijolite as in Fig. 1g (Sample MV12.SY02).

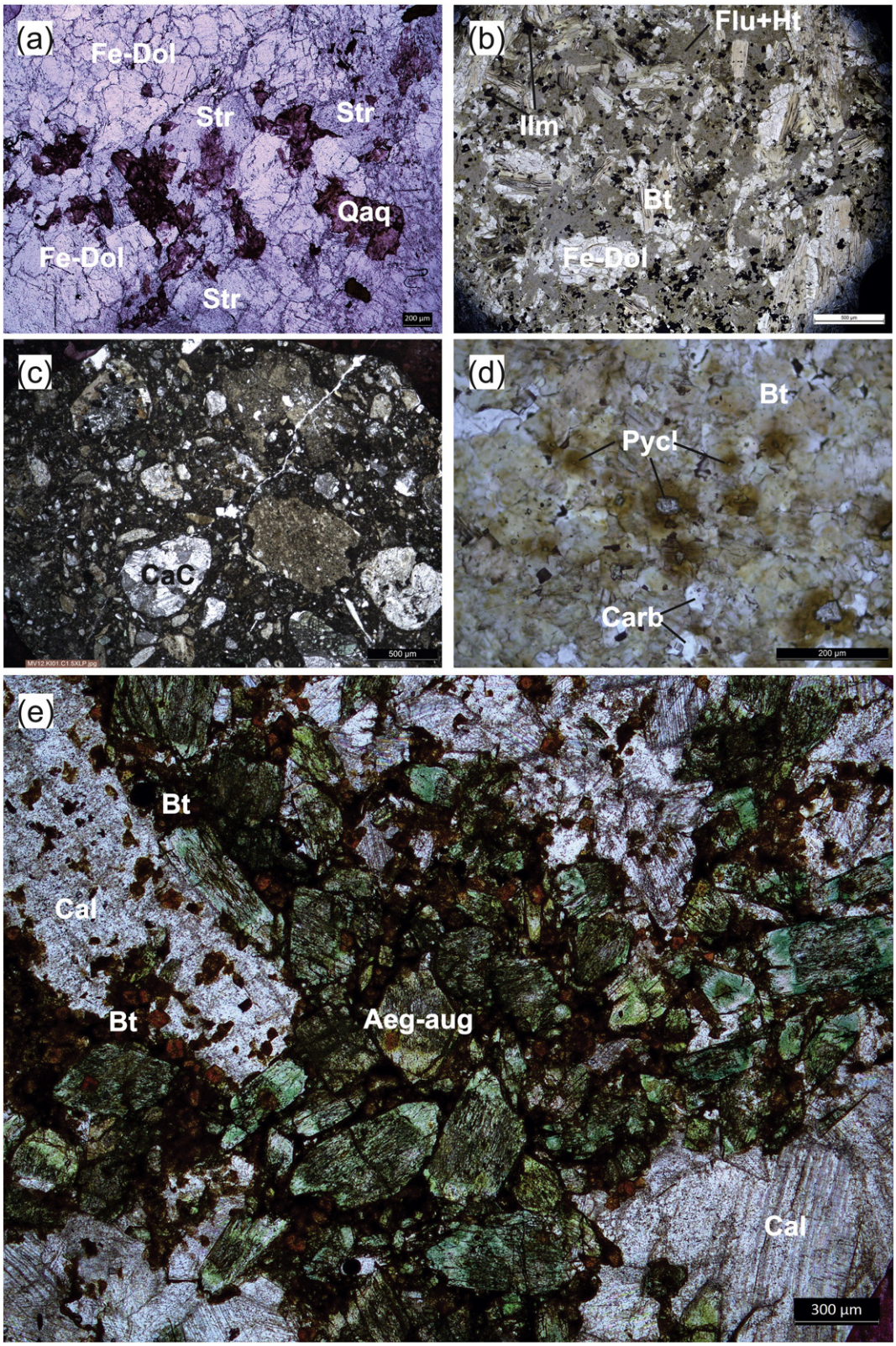

Fig. 4. Photomicrographs of silicocarbonatites showing mineral and texture relations. Photographs are in transmitted light unless otherwise stated. (a) Carbonate-rich part of a glimmerite breccia-type silicocarbonatite consisting of ferroan dolomite (Fe-Dol), strontianite (Str) and qaqarssukite-(Ce) (Qaq) pseudomorphing a pre-existing mineral (Sample LP12.UMBX01). (b) Lamprophyre-like silicocarbonatites showing kinked biotite booklets, like in many lamprophyres, and ferroan dolomite with magnetite in a matrix of dolomite, fluorite and secondary hematite (Sample MV13.DYK2). (c) Crossed polar view of the kimberlite-like silicocarbonatite showing rounded enclaves of calciocarbonatite and other ferromagnesian-rich rocks and minerals in a matrix of calcite, ferromagnesian minerals, biotite, partially resorbed pyrite and zircon (Sample MV12.KI01). (d) Biotite-rich (glimmerite) part of the glimmerite breccia-type silicocarbonatite showing a close up view of pyrochlore (Pycl) with metamict halos in biotite. The translucent mineral may include calcite, dolomite and strontianite (Carb) (Sample LP12.UMBX01). (e) Partially digested enclave of biotite clinopyroxenite in calciocarbonatite showing phenocrysts of aegirine–augite altered to biotite in a mass of calcite (Sample MV12.SICACB02).

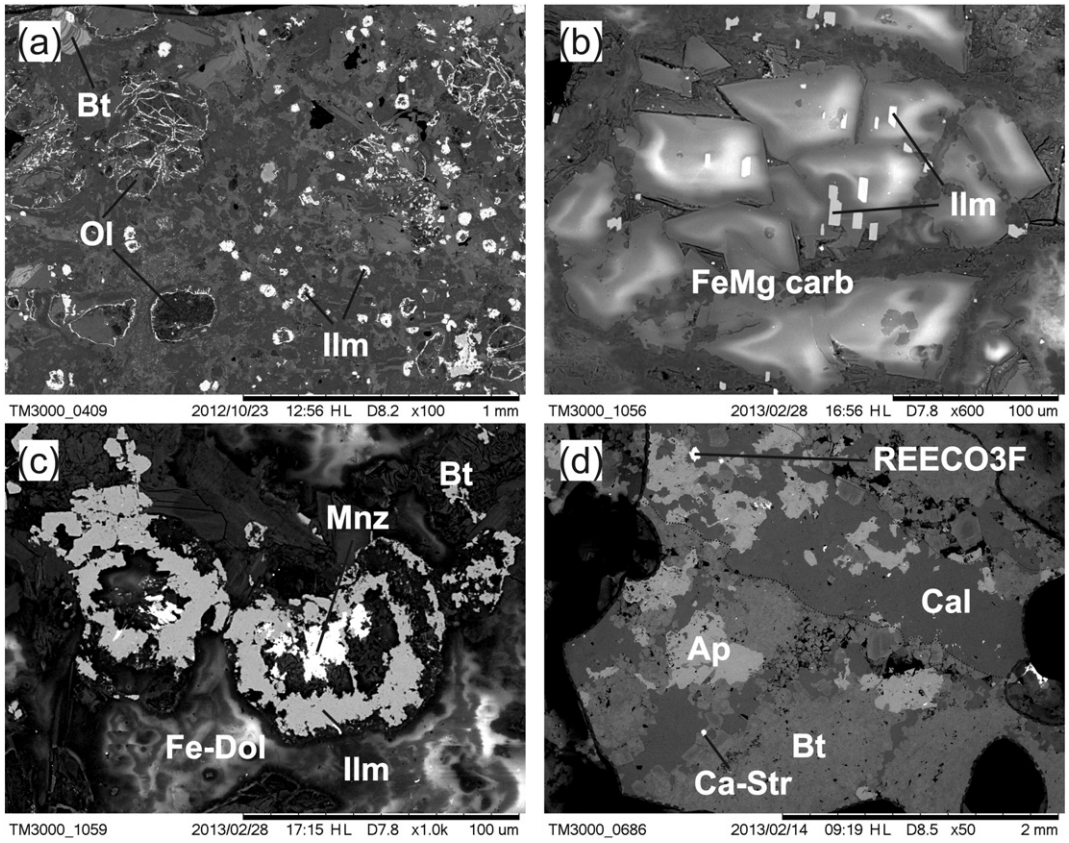

Fig. 5. Backscatter electron image of silicocarbonatites showing mineral and texture relations. (a) Hydrothermalized, lamprophyre-like silicocarbonatite with folded biotite booklets, olivine pseudomorphs (Ol) replaced with ilmenite, Fe–Mg carbonates and chlorite. The matrix hosts hydrothermal Fe–Ti oxides, biotite, apatite, monazite and pyrite (Sample MV12.HREE02A). (b) Close up view of an olivine pseudomorphin lamprophyre-like silicocarbonatite showing euhedral but secondary crystals of ilmenite and Mg–Fe carbonate in a matrix of ferroan dolomite and biotite (Sample MV12.HREE01). (c) Lamprophyre-like silicocarbonatite showing hydrothermal monazite, biotite, ilmenite in ferroan dolomite (Sample MV12.HREE01). (d) Glimmerite breccia-type silicocarbonatite showing the altered fluorapatite–strontianite biotitite cut by calcite, apatite and unidentified REE-bearing fluorocarbonate (Sample MV12.UMBX01).

stages of the petrogenesis. Primary oxides consist largely of ilmenite with some magnetite. Rare earth element-bearing phases including carbonates and fluorocarbonates (see Nadeau et al., 2015 for specific mineral names) as well as monazite-(Ce) and xenotime-(Y).

6. Whole rock composition

Major element analyses of representative whole rock samples of the Montviel alkaline complex are presented in Table A1 and Fig. 9. Silicate rocks (clinopyroxenites, melteigites, ijolites, melano- and leucosyenites and granites) range from about 35.6 to 73.4 wt.% SiO_2, 12.1 to 0.1 wt.% MgO (except for one with 25 wt.% CO_2), 1.4 to 17.1 wt.% CaO, 1.2 to 5.5 wt.% Na_2O, 1.0 to 6.2 WT.% K_2O and 1.3 to 17.8 $Fe_2O_3^{tot}$. The carbonatites (magnesiocarbonatites, calciocarbonatites, ferrocarbonatites and mixed carbonatites) range from 0.3 to 4.9 wt.% SiO_2, 0.2 to 13.6 wt.% MgO, 4.6 to 51.3 WT.% CaO, 0.1 to 1.9 WT.% Na_2O, 0.0 to 1.0 wt.% K_2O and 0.6 to 44.9 wt.% $Fe_2O_3^{tot}$. Silicocarbonatites have intermediate compositions and range from about 10.8 to 34.8 wt.% SiO_2, 9.6 to 16.4 wt.% MgO, 10.8 to 19.7 wt.% CaO, 0.2 to 3.3 wt.% Na_2O, 1.7 to 6.3 wt.% K_2O, and 12.7 to 14.6 wt.% $Fe_2O_3^{tot}$. The sample of polygenic breccia also has intermediate compositions with 15.3 wt.% SiO_2, 6.6 wt.% MgO, 29.1 wt.% CaO, 1.3 wt.% Na_2O, 2.5 wt.% K_2O and 12.0 $Fe_2O_3^{tot}$.

The nomenclature of carbonatite used herein follows that in Goutier (2006); Desharnais and Duplessis (2011) and Nadeau et al. (2015) and samples are plotted on the CaO–MgO–(FeO + MnO) ternary classification diagram of Woolley and Kempe (1989); Fig. 9b). The calciocarbonatites, magnesiocarbonatites and ferrocarbonatites fall within their fields. However, a sample of fluorite-rich ferrocarbonatite falls within the field of calciocarbonatite because of the large concentration of CaF_2. Mixed carbonatites fall within the field of ferrocarbonatites because they are dominated by Fe-bearing carbonate minerals (ankerite, ferroan dolomite, and siderite). The polygenic breccia has only 8.9 wt.% CO_2 and is not truly a carbonatite. It nevertheless plots within the field of ferrocarbonatites.

7. Biotite

7.1. Major element concentration

Biotite is ubiquitous at Montviel both in silicate and carbonatite rocks and displays highly variable textures and habits, i.e., coarse to aphanitic, green to brown, euhedral to anhedral, cumulate, disseminated and vein-shaped. Biotite was analyzed for major elements and Ti, Ce, F, Cl and S (Table A2). Cerium and S were always below the limit of detection of about 800 and 250 ppm, respectively. Chlorine was often detected with concentrations around 150–400 ppm, with a few data points at around 1000 ppm. Some biotite was chemically altered and returned low K_2O and/or high Na_2O or CaO and/or high FeO + MgO. These altered crystals were removed from subsequent calculations and diagrams.

A plot of TiO_2 vs F (Fig. 10a) highlights 3 distinct biotite populations: (1) high TiO_2–low F (TiO_2 2.5–3.5 wt.%; F 0–1 wt.%) present in clinopyroxenite, melteigite and ijolite; (2) high F and variable

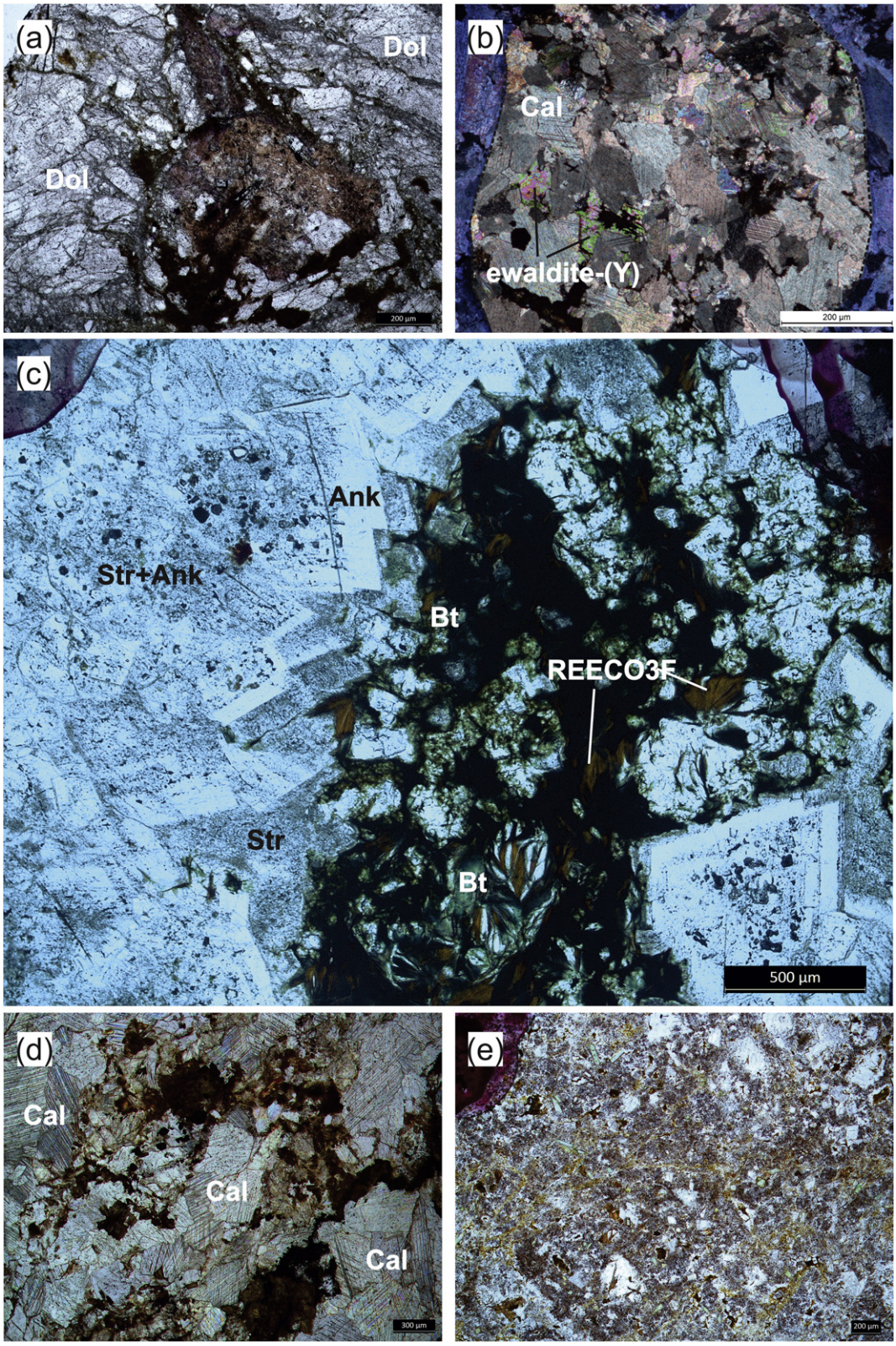

Fig. 6. Photomicrographs of carbonatites showing mineral and texture relations. Photographs are in transmitted light unless otherwise stated. (a) Hydrothermally altered and mineralized magnesiocarbonatite. Dolomite is strongly altered to Ba–Ca-rich strontianite, Ba-rich dolomite, fluorite, pyrite and sphalerite (Sample MV12.FECB01AB). (b) Crossed polar view of calciocarbonatite with calcite and ewaldite-(Y) (Nadeau et al., 2015) (Sample MV12.HREE02B). (c) Comb-like, ankerite–strontianite assemblage in ferrocarbonatite showing open space crystallization of biotite and Ba–REE fluorocarbonate (Sample MV12.FECB02). (d) Calciocarbonatite showing decussate textured calcite cut by veinlets of clear barytocalcite and strontianite, reddish qaqarssukite-(Ce) and ewaldite-(Y), and opaque sphalerite and galena (Sample MV12.LATE1). (e) Polygenic breccia displaying a strongly altered matrix made of fluorapatite and calcite, with strontianite, aegirine–augite, biotite, qaqarssukite-(Ce), sphalerite and clasts of carbonatites (Sample MV12.HREE03).

TiO_2 (F >1 wt.%) present in silicocarbonatites, calciocarbonatites and polygenic breccias; and (3) low TiO_2–low F (TiO_2 <1 wt.%; F <1.5 wt.%) present in all lithologies except silicocarbonatites. The third population can be subdivided into 2 sub-types, with silicate rock biotites at lower F (<1 wt.%) and carbonatite biotites clustering tightly at higher F concentrations (mostly 1–1.5 wt.%). Note that the silicocarbonatites only have high-F biotite and that biotites from the silicate rocks are totally distinct from those of carbonatites. On a plot of Mg# vs F (Fig. 10b), biotite from the silicate rocks plots on a distinct trend from those in carbonatites, with the exception of biotite from the granites and polygenic breccias, which plots between the 2 trends at low Mg# and F.

7.2. Crystallization temperature

Biotite crystallization temperatures were calculated using the algorithm by Henry et al. (2005). Although the geothermometer was initially developed for ilmenite- or rutile-saturated graphitic metapelites equilibrated at 400–600 MPa and 480–800 °C, other studies have shown that it can be applied to conditions different than those for which it was first calibrated (e.g., Erić et al., 2007). Given that the Ti saturation surface in Mg/(Mg + Fe)-temperature-Ti space is similar under magmatic conditions (e.g., Patiño-Douce, 1993), we have attempted to apply it to Montviel. Ilmenite and/or rutile, as well as other Ti-bearing phases such as perovskite, titanite and joaquinite are common at Montviel (Fig. 8). Nevertheless, differences exist between biotites used for the calibration of the model and those at Montviel, the most important difference being that Henry et al. (2005) metapelites were peraluminous whereas rocks from Montviel are metaluminous to peralkaline. Hence, care must be taken when considering biotite temperatures on an absolute basis. At Montviel, the calculated biotite crystallization temperatures range from 774 to 368 ± 12–24 °C (Table A2). On a plot of temperature vs TiO_2, the biotites from silicate rocks still plot apart from those from carbonatites (Fig. 10c). Biotites from clinopyroxenites cluster tightly at relatively high temperature (around 650–700 °C) whereas biotite from carbonatites range widely from high to low temperature (750–380 °C). These temperatures are consistent with a metasomatic origin for all biotites.

7.3. REE concentration

The laser ablation of biotite for REE analyses (Table A3) proved to be challenging and extreme care was taken to avoid inclusions of mineral such as pyrochlore, rutile and zircon. Chondrite-normalized REE patterns generally show a smooth negative slope from 1 to 100 times chondrite for La to 0.1–10 times chondrite for Lu (Fig. 11). However, most of the biotites plot in the center of the data envelope shown in gray.

REE element profiles for biotites from the clinopyroxenites have highly variable REE contents that range from an essentially flat 1-time-chondrite pattern to an enriched pattern at 100 times chondrite for LREE, MREE values near 10–100 times chondrite and HREE near 10 times chondrite.

In melteigite and ijolite, the biotites are very similar and cluster tightly in the center of the envelope near intermediate values, showing an LREE enrichment of 10–20 times chondrite, mild negative slopes, and HREE values near 1 time chondrite. The granites hosts biotites which are among the most REE depleted, with La around 1–10 times chondrite and HREE values around 0.1–1 times chondrite.

Biotites from silicocarbonatites vary widely from the most REE depleted to some of the most REE enriched values, similar to biotite in the clinopyroxenites. However, these biotites have a relatively steep LREE-enriched slope, unlike those of the clinopyroxenites and polygenic breccias. LREE varies from 1 to 100 times chondrite, down to 0.1–5 times chondrite at Y, with the heavier HREE (Y to Lu) displaying strongly negative to mildly positive slopes.

Most rare earth element patterns for biotite from the calciocarbonatites and ferrocarbonatites are very similar to those of the silicocarbonatites and clinopyroxenites that are enriched in REE. Apart from one which is flat and depleted, most are enriched in LREE with 1–100 times chondrite, down to Y values around 0.2–2 and remain strongly negative from Y to Lu. Biotite from the matrix of the polygenic breccias is relatively REE enriched and displays mildly negative to nearly flat, concave downward patterns with medium to heavy REE enrichment, similar to, but even more enriched than some found in clinopyroxenites.

8. Clinopyroxene

Clinopyroxene was analyzed for major elements and ranged in composition from augite to aegirine (Table A4). Pure augite was rare and found exclusively in relatively fresh clinopyroxenite and melteigite. Most of the clinopyroxene was aegirine–augite, found in clinopyroxenites, melano- and leucosyenites, ijolites and silicocarbonatites. A few pure aegirines were identified in melteigites and ferrocarbonatites.

9. Tectosilicates

X-ray diffraction (Table A7), SEM-EDS and an electron microprobe were used to help distinguish and characterizing the various feldspars, feldspathoids, zeolites and pseudo-zeolites present at Montviel (Table A5). In general, nepheline, sodalite, cancrinite and analcime were observed in clinopyroxenites, melteigites and ijolites whereas microcline and plagioclase were found in melanosyenites, leucosyenites and granites. Albite was present in all feldspatoidal and K feldspar bearing rocks.

10. The Sm–Nd isotope geochemistry of biotite and aegirine–augite

Neodymium isotope ratios from metasomatic biotite and aegirine–augite do not form an isochron and yield ε_{Nd} (1894 Ma) values ranging from +3.4 to −3.0 (Fig. 12, Table A6). This range of ε_{Nd} values indicates open system behavior as a result of mixing between depleted and enriched components. The measured $^{143}Nd/^{144}Nd$ ratios are bracketed between two fitted isochrons; a 1.894 Ga isochron representing the U–Pb age of the complex (David et al., 2006) and a 1.0 Ga isochron selected arbitrarily that closes the bracket. Both isochrons were drawn using an initial $^{143}Nd/^{144}Nd$ ratio of 0.5105 to represent the depleted mantle at 1.9 Ga. Biotite and aegirine–augite from clinopyroxenites have ε_{Nd} values of +3.4 and +2.0, respectively. Aegirine–augite from ijolite has a moderately value of +0.8. The two biotites from glimmerite breccias have values of +2.6 and −2.3. The biotite–apatite mixture from polygenic breccia matrix and aegirine–augite from calciocarbonatite have negative values of −1.5 and −3.0, respectively.

11. Discussion

Cross-cutting relationships observed in outcrops and drill cores provide the most compelling evidence that the alkaline complex evolved from clinopyroxenites to more evolved silicate rocks, silicocarbonatites and carbonatites (Goutier, 2006; Nadeau et al., 2015). The petrographic observations of mineralogical and textural relationships presented here suggest that metasomatism was omnipresent throughout the evolution of the magmatic–hydrothermal system. Biotite major element geochemistry documents distinct compositions (metasomatic events) for silicate rocks and carbonatites (Fig. 10), indicating that silicate rocks were not metasomatized by carbonatite fluids. The Sm–Nd isotopes from biotites and aegirine–augites demonstrate that the fluid system was

open and fluid mixing occurred between depleted and enriched fluid sources. Hereafter, a 'fluid' refers to a low density, low viscosity phase, distinct from silicate and carbonatite melts, and composed of volatile species (H_2O, CO_2, H_2S, HCl, etc.), metals (Na^+, K^+, $Fe^{2+\text{ or }3+}$, REE^{3+}, etc.) and ligands (e.g., Cl^-, HS^-, CO_3^{2-}, etc.). Depending on pressure, temperature and composition, this fluid might have been in a supercritical state, at the liquid or at vapor state.

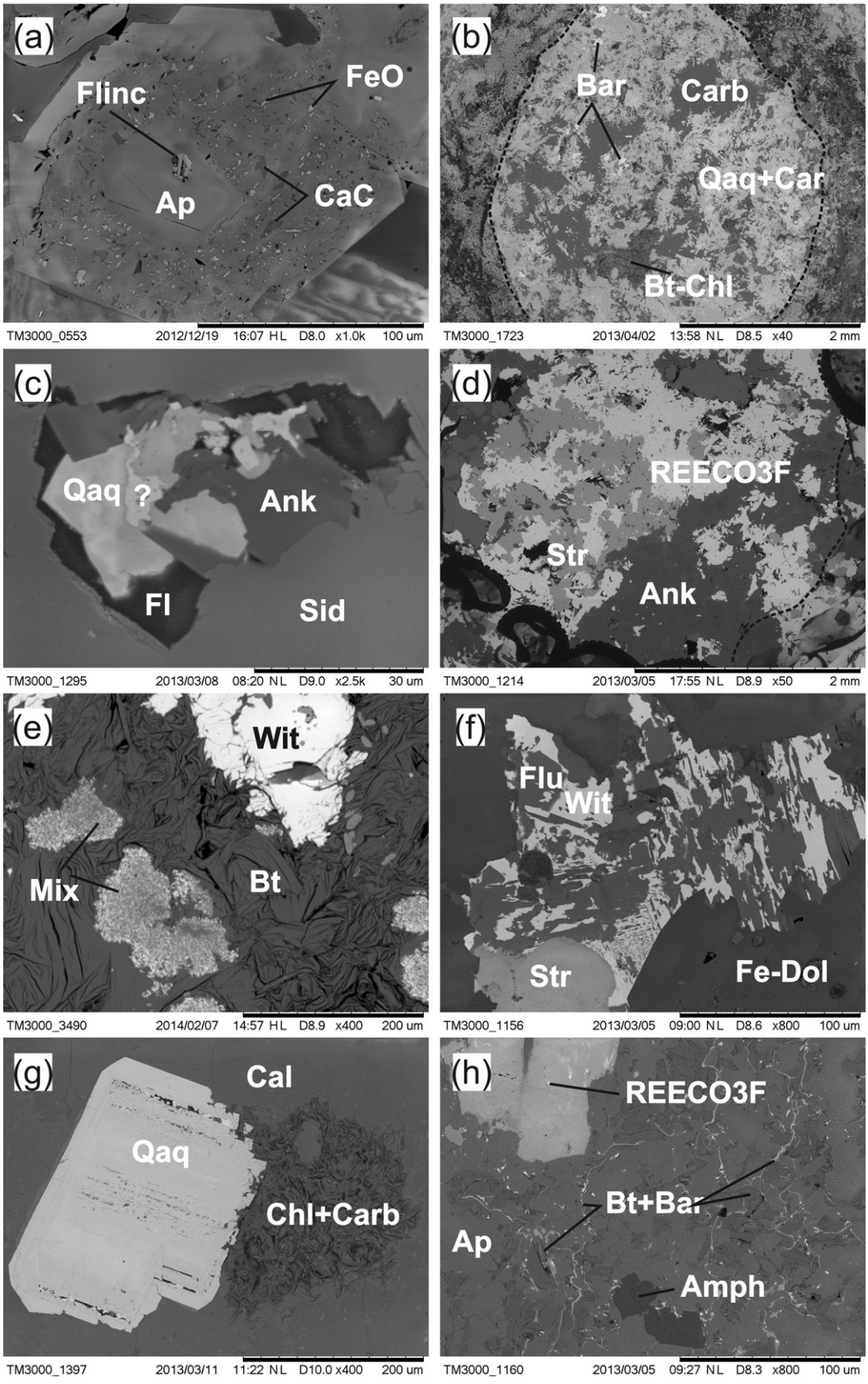

11.1. Metasomatism

11.1.1. The effect of metasomatism

The evolution of the clinopyroxenites to melteigites and ijolites is typically reflected in the relative increase in nepheline and sodalite and the resulting decrease in clinopyroxene (e.g., Washington, 1901). In general, nepheline and sodalite are higher temperature, magmatic phases (Tuttle and Smith, 1958; Tomisaka and Eugster, 1968), cancrinite forms at lower temperature and is magmatic or hydrothermal (Sirbescu and Jenkins, 1999) and analcime forms at very low temperature and is usually metasomatic or low grade metamorphic (Neuhoff et al., 2004). However, Drüppel et al. (2005) showed that Na-rich magmatic fluids can convert nepheline to sodalite and that nepheline can react with saline fluids to produce sodalite, cancrinite and analcime (Fall et al., 2007).

The Na–K–Fe metasomatism at Montviel is evident in the replacement of augite by aegirine–augite and aegirine by Na-Fe^{3+}-rich fluids (Figs. 2a–c and 3b; see also Le Bas, 1977):

Augite → Aegirine

$$Ca\left(Mg, Fe^{2+}\right)Si_2O_6 + Fe^{3+} + Na^{+} \rightarrow NaFe^{3+}Si_2O_6 + 0.5Mg^{2+} + 0.5Fe^{2+} + Ca^{2+} \quad \text{(reaction 1)}$$

Petrographic textures also suggest that nepheline + analcime (Figs. 2f and 3e) and nepheline + cancrinite (Fig. 3b) formed after metasomatic recrystallization of an unidentified precursor. These same fluids provoked the albitization of plagioclase in the syenites and granites (Fig. 2h) and the formation of albite through alteration of nepheline or analcime (Fig. 3c) in the clinopyroxenite–melteigite–ijolite series via the following reactions:

Nepheline → Albite

$$2(Na_{0.5}K_{0.5})AlSiO_4 + Na^{+} + 4SiO_2 \rightarrow 2NaAlSi_3O_8 + K^{+} \quad \text{(reaction 2)}$$

Analcime → Albite

$$NaAlSi_2O_6 \cdot H_2O + SiO_2 \rightarrow NaAlSi_3O_8 + H_2O \quad \text{(reaction 3)}$$

The metasomatizing fluid replaced the magmatic biotite with lower temperature biotite (Figs. 2a–c and 10c) and likely recrystallized high temperature potassium feldspars (sanidine, orthoclase) in the syenites to microcline (Fig. 2h; Table A7) as has been documented in other alkaline complexes (Henry et al., 2005; Pirajno, 2013).

The role of Fe in the metasomatic fluid is evident from the aegirinization of augite (reaction 1) and from the fact that all carbonates with magmatic textures at Montviel are either calcite or dolomite whereas ferroan–dolomite, ankerite, siderite, but also biotite, aegirine–augite and aegirine were hydrothermal or metasomatic. This suggests that ferrocarbonatites were produced from calciocarbonatites by fractional crystallization and Fe-metasomatism.

11.1.2. Nature and origin of the metasomatic fluids

The clinopyroxenites represent the first magmas injected at Montviel, although the presence of olivine pseudomorphs in some rocks suggests that the original compositions may have been olivine clinopyroxenitic or wherlitic magmas. Biotite in the clinopyroxenites crystallized from – or equilibrated with – a fluid, returning model crystallization temperatures of 640–700 °C (Fig. 10c; Henry et al., 2005). Such fluid temperatures in clinopyroxenite magma simply subsolidus conditions and Nd isotope compositions of the biotite and aegirine–augite samples suggest that cooling was driven by mixing with external fluids, which is consistent with the rock's alteration textures (Fig. 1a–c). For example, biotite and aegirine–augite from the clinopyroxenite yield ε_{Nd} values of +2.0 to +3.4, whereas the modeled depleted mantle at ca 1.9 Ga would have had an ε_{Nd} value of about +6 (assuming $^{147}Sm/^{144}Nd_{DM} = 0.21362$; Jacobsen, 1988). The lower Nd isotope compositions of the clinopyroxenite minerals reflect either crustal contamination or an enriched mantle source. The presence of an even lower ε_{Nd} value (+0.8) in aegirine–augite in the ijolite supports the presence of a crustal contaminant. Given that the minerals are hydrothermal or metasomatic, we argue that mixing occurred between fluids originating from the depleted mantle and the enriched crust.

Biotites from the clinopyroxenite have flat to mildly negative REE patterns extending between 1 and 100 times chondrite (Fig. 11). It is possible to calculate the composition of fluid that formed these biotites using mica/fluid partition coefficients for REE in basanite (Adam et al., 2014). These calculations yield a fluid with approximately 5 to 300 ppm LREE, 0.05 to 24 ppm MREE and 0.1 to 30 ppm HREE (Fig. 13), which is 2 orders of magnitude lower in LREE to 1 order of magnitude lower in HREE than was measured in fluid inclusions from the Kalkfeld and the Okorusu carbonatite complexes, Namibia (Bühn and Rankin, 1999; Bühn et al., 2002).

Cross-cutting field relations and core samples as well as major element geochemistry (Fig. 9) suggest that the clinopyroxenites were comagmatic with – and followed by – melteigites and ijolites via fractional crystallization. The fluids accompanying each successive magma were likely in disequilibrium with the preceding magma/fluid because of the combined fractional crystallization and mixing with external fluids, ultimately leading to the metasomatism of the units.

Model crystallization temperatures calculated for the biotite compositions of the melteigites and ijolites 670–770 °C (Fig. 10c) are similar to those of the clinopyroxenites. However, the REE contents of the biotites from melteigites and ijolites have flat to mildly negative REE patterns extending between 1 to 10 times chondrites (Fig. 11) that yield model fluid compositions of 30 to 80 ppm LREE, 0.1 to 2.4 ppm MREE and 0.7 to 3.8 ppm HREE. The REE profiles of these fluids, although similar in form to those of the clinopyroxenites are overall more depleted in all REE (Fig. 13).

Two biotites from the carbonatites returned temperatures of 470 °C and 485 °C, representing high but subsolidus temperature conditions for the carbonatite magmas. Both the metasomatized calciocarbonatites and ferrocarbonatites contain biotite with similar REE contents, varying from 100 times chondrites LREE to chondrite-like HREE values. Based on mica/fluid partition coefficients for REE (Adam et al., 2014), the biotite-bearing fluid would have had 5 to 440 ppm LREE, 0.2 to 13 ppm MREE and 0.5 to 3 ppm HREE, values which are about 2–3 orders of magnitude lower than fluid inclusions from the Kalkfeld and the Okorusu carbonatite complexes, Namibia (Fig. 13) (Bühn and Rankin, 1999; Bühn et al., 2002).

All calculated fluids have REE concentrations about 1 to 3 orders of magnitude lower than fluid inclusions from the Kalkfeld and the

Fig. 7. Backscatter electron image of carbonatites showing mineral and texture relations. (a) Euhedral fluorapatite displaying a fresh outer rim, an inner rim filled with numerous micron-size inclusions of carbonatite melt, iron oxides, hydroxylapatite and numerous other unidentified inclusions, and a relatively fresh core with a single opened fluid inclusion with Fe-rich and Ca–Na–Si-rich minerals (iron oxide and plagioclase?). The apatite is in calciocarbonatite (Sample LP12.CACB01A). (b) Late, mixed carbonatite sample showing a hydrothermal qaqarssukite–carbocernaite–barite assemblage with unidentified Ca–Fe–Mg carbonates and chloritized biotite (Sample MV13.RAMP3). (c) Siderite-hosted inclusion from a ferrocarbonatite, consisting of fluid (now void), daughter ankerite and qaqarssukite-(Ce) cut by an unidentified Ca–Fe–Th–Y silicate (?) (Sample MV12.CAFECB02). (d) Mineralized part of a ferrocarbonatite showing hydrothermal Ba–REE fluorocarbonate (kukharenkoite or huanghoite) and strontianite in metasomatic ankerite (Sample MV12.FECB02). (e) Close-up view of a hydrothermally altered zone of LREE-bearing ferrocarbonatite showing Sr-bearing witherite (Wit), biotite and a complex sub-micron scale mix of monazite, iron oxides and carbonates (Mix) (sample MV13.FECL2). (f) Ferrocarbonatite showing what could be symplectitic crystallization of witherite and fluorite in a hydrothermally altered zone of a ferrocarbonatite (Sample LP12.CAFECB01A). (g) Late, mixed carbonatite sample showing complexly zoned qaqarssukite-(Ce). Partially dissolved qaqarssukite in contact with chlorite and carbonates (sample MV12.LATE2). (h) Polygenic breccia consisting mostly of fluorapatite and calcite, cut by numerous late veinlets of biotite and barite. Clasts of Sr–Ca–Ba–Na–REE carbonates (burbankite-(Ce) or carbocernaite-(Ce)) and fluoropotassic amphibole are present (Sample MV12.MBX04).

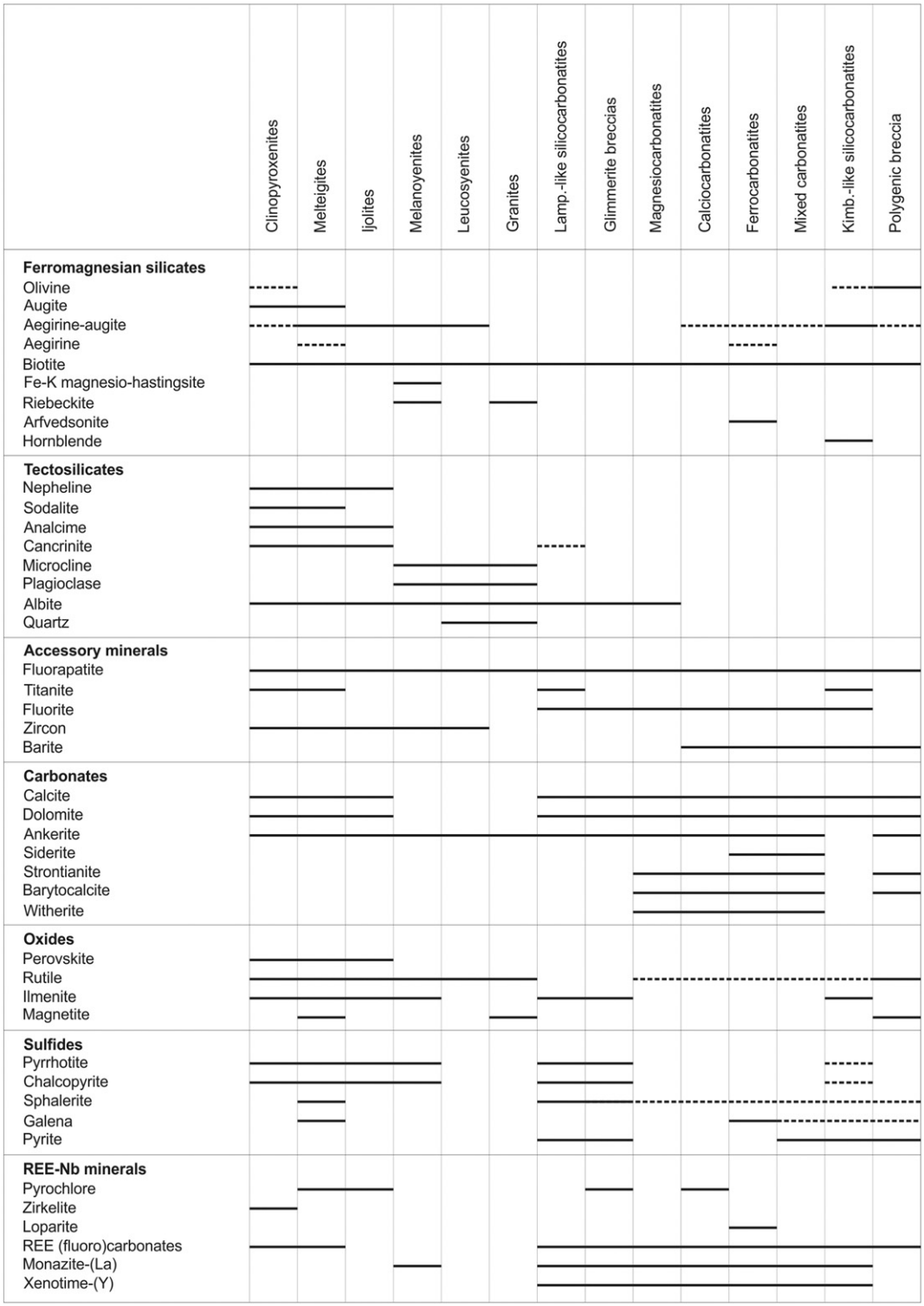

Fig. 8. Mineral paragenesis based on field and drill core relationships, optical and scanning electron microscopy, X-ray diffraction and electron microprobe results.

Okorusu carbonatite complexes, Namibia (Fig. 13) (Bühn and Rankin, 1999; Bühn et al., 2002). Assuming that equilibrium was maintained between biotite and the fluid, this could result from: (1) the use of partition coefficients that are not applicable to conditions at Montviel, (2) biotites not crystallizing from the REE-bearing fluids, or (3) Montviel REE ore depositing from a fluid which had much less REE than that from the Kalkfeld and the Okorusu carbonatite complexes. Hypothesis (2) is ruled out as many of the analyzed biotites were in contact with – or very close to – REE-bearing fluorocarbonates (Fig. 6c). Given the extremely large variations in REE concentrations between fluid inclusions from the Kalkfeld and Okorusu carbonatites, i.e., 2.4 ± 1.3 wt.% REE (n = 9), and the model fluids presented here, i.e., up to about 450 ppm (fluid from Bt in ferrocarbonatite ore), we favor the first hypothesis according to which the available partition coefficients are not applicable and the fluid must have had REE concentrations higher than that calculated. One calcite-hosted melt inclusion from calciocarbonatite at Montviel returned 186 ppm REE (Nadeau et al., 2015) and the fluid in equilibrium with biotite from calciocarbonatite,

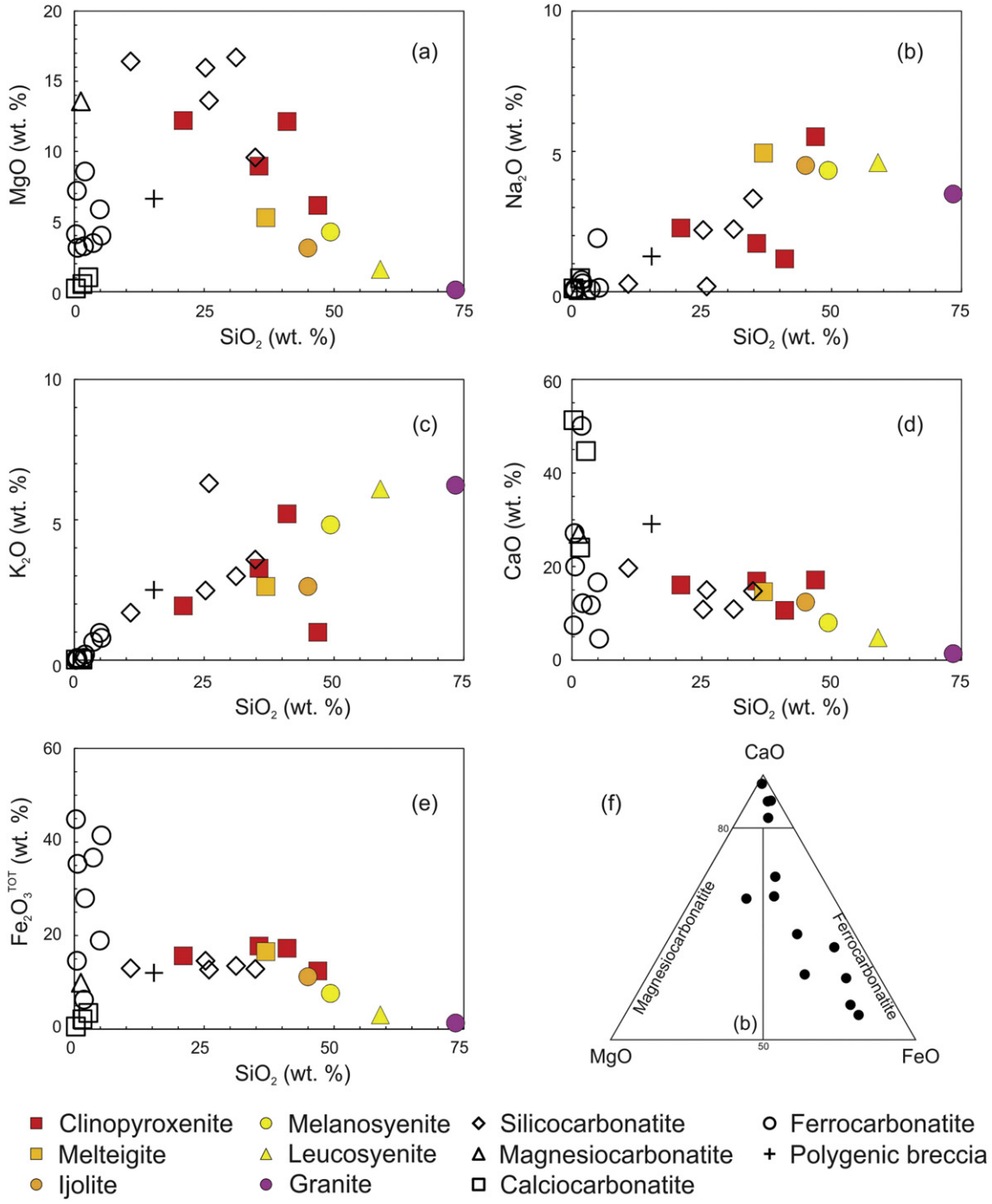

Fig. 9. Bulk rock major element concentrations (Table A1). (a) MgO vs SiO_2 plot discriminates silicate rocks at high SiO_2 from carbonatites at low SiO_2. Silicocarbonatites plot at intermediate values. (b) Ternary CaO–MgO–FeO + MnO classification diagram for carbonatites.

based on partition coefficients used herein, would have 160 to 220 ppm REE. This suggests a fluid/melt partition coefficient near unity, which is low considering that all carbonatite-hosted REE deposits are hydrothermal (except Mountain pass, Chakhmouradian and Zaitsev, 2012) and further supports that the 1st hypothesis.

11.1.3. Silica saturation

The presence of a thermal divide along the albite-K feldspar in the $NaAlSiO_4$–$KAlSiO_4$–SiO_2system prevents the evolution of silica-undersaturated magmas to silica-saturated rocks via fractional crystallization (Bowen, 1928). Previous studies (Landoll and Foland, 1996) have shown that the association of essentially coeval quartz-saturated syenites and granites with silica-undersaturated syenites as is observed at Montviel reflects the assimilation of silica-saturated crustal rocks and/or fluids, combined with fractional crystallization. The subsolidus temperatures (620–370 °C) recorded in biotites from the granites and other lithologies indicate that the biotites re-equilibrated with – or crystallized from – late metasomatizing fluids. The low REE concentrations in biotites from the granites indicate that the contaminating fluid had less overall REE concentrations than the melteigites, ijolites and melanosyenites. Initially the Montviel complex thus consisted of a REE-rich, silica-undersaturated magmatic hydrothermal system that mixed with REE-poor, silica-saturated rocks and fluids. The resulting mixture led to Na–K–Fe metasomatism as indicated by the presence of

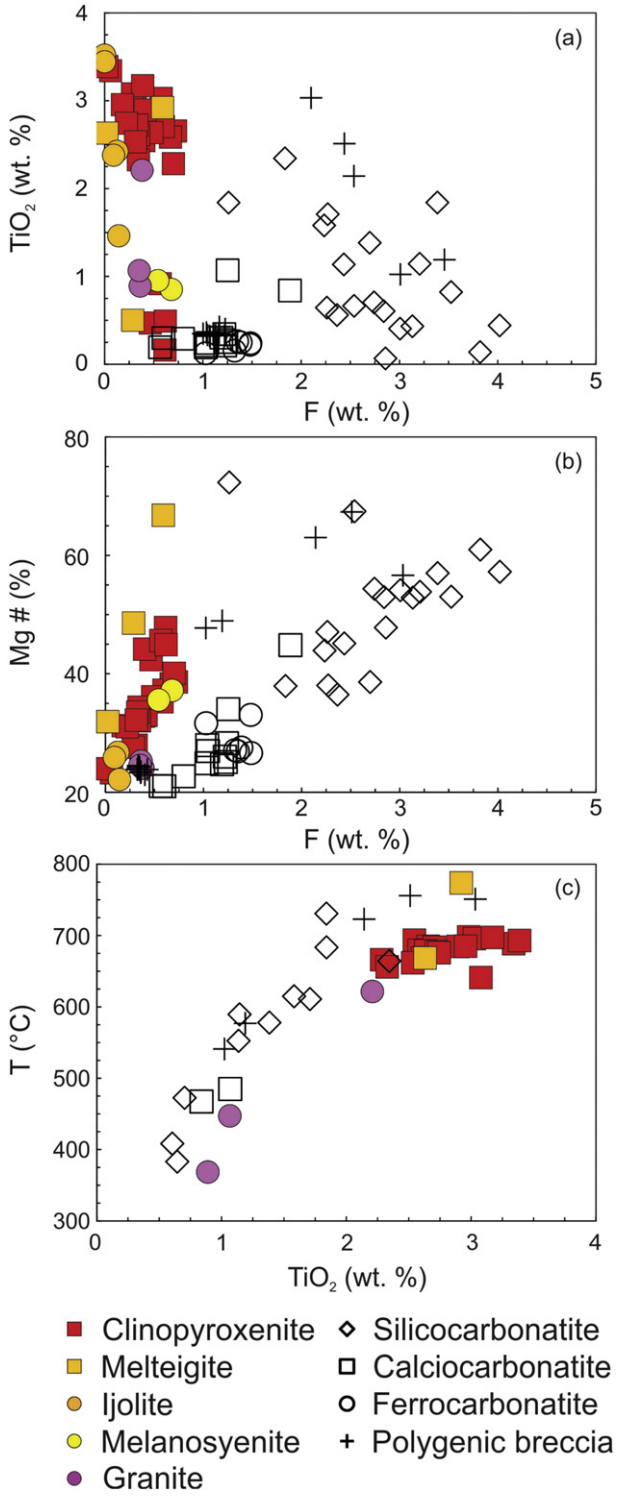

Fig. 10. Biotite major element concentrations (Table A2). (a) Concentration of TiO_2 vs F. (b) Mg# vs F. (c) Model crystallization temperature vs TiO_2 (Henry et al., 2005).

aegirine–augite, riebeckite, albite (Ab_{86} to Ab_{100}), biotite, ankerite and microcline in leucosyenites and granites.

11.2. Magmatic evolution

11.2.1. Multiple mantle pulses

Field and drill core cross-cutting relationships, mineralogy, bulk rock composition and ε_{Nd} values for mineral separates indicate that the clinopyroxenites represented the first injection of consanguineous magmas and fluids which gradually evolved to melteigites, ijolites and melanosyenites via fractional crystallization, fluid mixing and metasomatism, and further evolved to leucosyenites and granites by a combination of the latter and assimilation of silica-saturated wall rocks.

The early lamprophyric and the late kimberlitic silicocarbonatites are 'true' silicocarbonatites in the sense that they contain 10–50% magmatic carbonate minerals which were co-magmatic with the other (silicate, etc.) minerals present in the rock. By contrast, the glimmerite breccias are not 'true' silicocarbonatites as they formed by infiltration of calciocarbonatite melt into glimmerites.

Chondrite-normalized REE patterns for silicocarbonatites are very similar to those of the clinopyroxenites but different from those from the melteigites, ijolite and granites indicating that the silicocarbonatites were not products of the clinopyroxenite–melteigite–ijolite series. In fact the lamprophyric silicocarbonatites cut through all silicate rocks indicating a subsequent magmatic pulse. Although melteigites and ijolites did crystallize some calcite and dolomite, the silicocarbonatites represent a large increase in the amount of magmatic calcite and dolomite and hydrothermal ankerite. This suggests that the clinopyroxenite–melteigite–ijolite series and accompanying syenites and granites were followed by a subsequent pulse of lamprophyric silicocarbonatites.

Two biotite fractions from the glimmerites yielded ε_{Nd} values of +2.6 and −2.3. These values again demonstrate that depleted mantle-derived fluids of the Montviel complex interacted with crustal fluids resulting in the observed variation in the Nd isotope compositions. The subsolidus model crystallization temperatures (730–380 °C) obtained for the biotites in the glimmerites suggests that this interaction continued after solidification of the complex through hydrothermal means.

The lamprophyric silicocarbonatites and glimmerite breccias represent a second pulse of magmas that cut through the previous melteigite–ijolite–syenite series and evolved to magmatic calciocarbonatites and metasomatic ferrocarbonatites. A 3rd pulse of repeated mantle injections led to a mixture of dykes, pods and lenses of silicocarbonatites, calciocarbonatites and ferrocarbonatites.

The mixed carbonatites were followed by the intrusion of a 50 m wide dyke of kimberlitic silicocarbonatite that cross-cut all earlier lithological units and contains clasts of these lithologies (Fig. 4c). The dyke consists of fresh olivine and metasomatic aegirine–augite and biotite and the brecciated texture of the rock testifies to the highly energetic emplacement of this unit.

The polygenic breccia is the last unit to be emplaced during the evolution of the alkaline complex. Like the preceding kimberlitic silicocarbonatite dyke, it contains olivine and it is highly brecciated and metasomatized (Figs. 6e, 7h, 8, 10, and 12). A mineral separate of mixed biotite returned an ε_{Nd} value of −1.5 and biotites from the polygenic breccia returned model crystallization temperatures of 750–540 °C (Fig. 10c), underlining again the role of low temperature crustal metasomatism in the evolution of the complex. Given that the kimberlitic silicocarbonatite and the polygenic breccia were the last two units to be emplaced and that both are brecciated, it is highly probable that the kimberlitic silicocarbonatite magma triggered the explosion which created the polygenic breccias. Thus, magmatic–hydrothermal activity at Montviel terminated as a violent, diatreme-making eruption rooted in the crust and the crustal fluids signature suggest this explosion might have been phreatomagmatic.

The polygenic breccias contain the HREE-enriched ore zone (Nadeau et al., 2015) and biotites from their matrix point toward a fluid enriched in HREE (Figs. 11–13). This suggests that the mixture of an initially mantle/magmatic fluid with crustal fluids appears to have preferentially remobilized the LREE and enriched the polygenic breccias in HREE.

11.2.2. Immiscibility and unmixing

Whether or not carbonatites result from immiscibility and unmixing of silicate and carbonate melts is an ongoing debate and results generally tend to show that it is possible but not always the case (Kjarsgaard

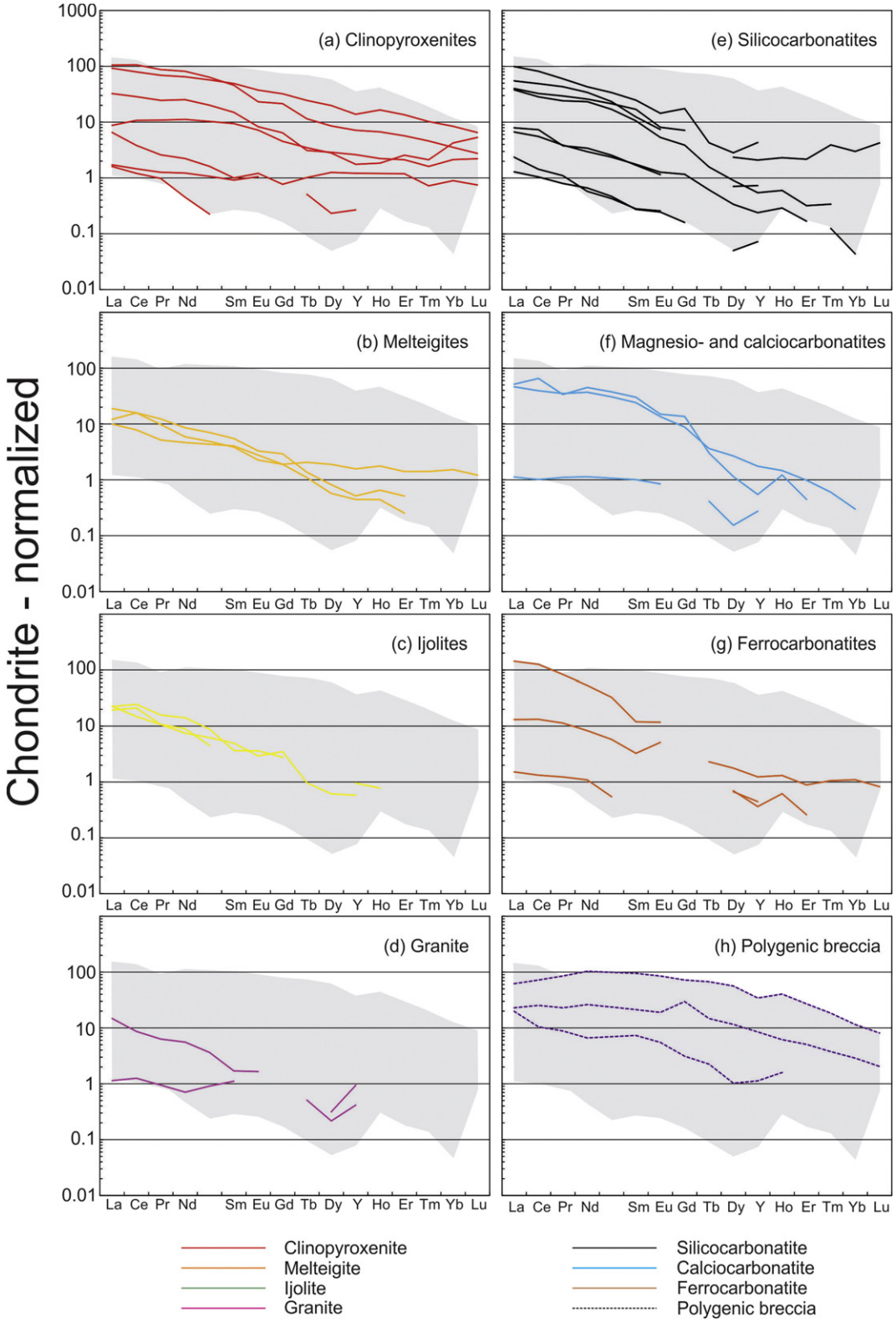

Fig. 11. Chondrite-normalized REE patterns for biotites (Table A3). The gray envelope represents the area covered by all biotites from Montviel. Chondrite data are from Sun and McDonough (1989).

and Hamilton, 1989; Wyllie et al., 1989; Gittins, 1989; Bell, 1998; Lee and Wyllie, 1998; Brooker and Kjarsgaard, 2011; Pirajno, 2015). At Montviel, clinopyroxenites first evolved toward melteigite–ijolite–syenite compositions and were subsequently cut by a second pulse of magmatic–hydrothermal activity represented by silicocarbonatites and carbonatites.

There appears to have been at least 3 end members for the metasomatic fluid. The first fluid was associated with the clinopyroxenites and other silicate rocks and was distinct from the second fluid, which was associated with silicocarbonatites and carbonatites. Both of these fluids displayed Nd-isotope ratios suggesting that they originated from depleted regions of the mantle

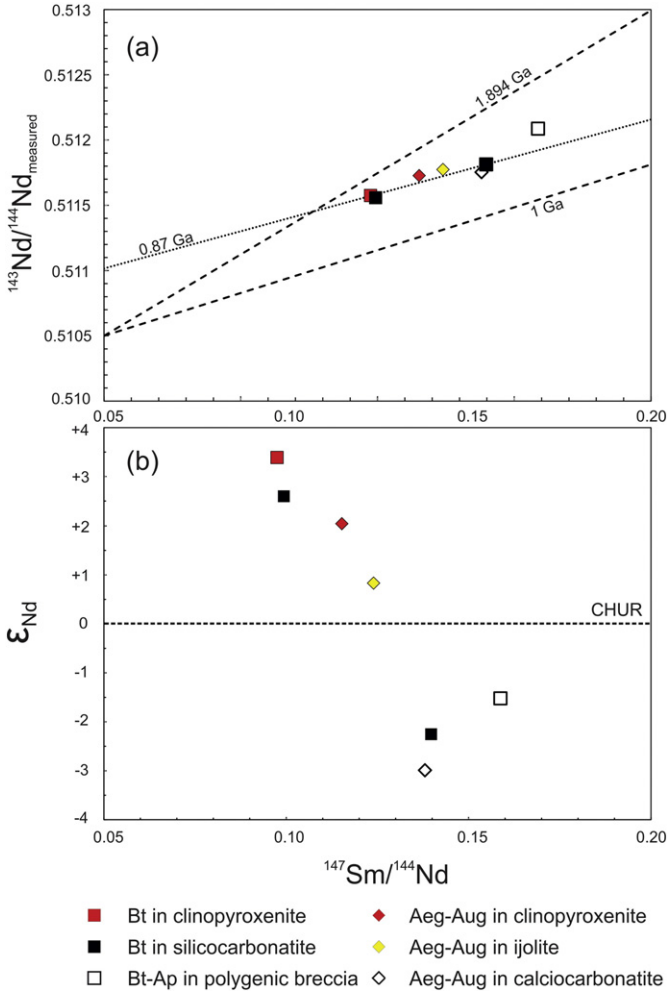

Fig. 12. $^{143}Nd/^{144}Nd_{measured}$ (a) and ε_{Nd} (b) vs $^{147}Sm/^{144}Nd$ for metasomatic biotite and aegirine–augite from Montviel. The measured $^{143}Nd/^{144}Nd$ ratios are bracketed between two fitted isochrons; a 1.894 Ga isochron representing the U–Pb age of the complex (David et al., 2006) and a 1.0 Ga isochron that closes the bracket. Both isochrons were drawn using an initial $^{143}Nd/^{144}Nd$ ratio of 0.5105 to represent the depleted mantle at 1.9 Ga.

and subsequently mixed with a third fluid originating from enriched regions of the crust.

Since true silicocarbonatites (lamprophyric and kimberlitic) display mineralogy and chemical compositions that are intermediate between clinopyroxenite and carbonatites, we argue that the carbonatites did not form by partial melting of pre-metasomatized and carbonated mantle (Bell and Blenkinsop, 1989), but instead resulted from the evolution of clinopyroxenites, which host calcite and dolomite, and silicocarbonatites. Nevertheless, carbonatites were separated from silicate magmas at some point during this evolution so immiscibility cannot be ruled out. The exact process by which the lamprophyrice silicocarbonatite evolved to a calciocarbonatite remains unconstrained.

11.2.3. Redox and pH

Silicate and carbonatite magmas at Montviel were dominated by pyrrhotite as the sulfide-, and ilmenite as the oxide liquidus phases, which shows that the system was relatively reduced. Pyrrhotite and chalcopyrite were more abundant in primitive silicate magmas and silicocarbonatites whereas sphalerite and galena became more concentrated in silicocarbonatites and carbonatites (Fig. 8). Petrographic relations suggest that these sulfides might have resulted from sulfide melt immiscibility (Fig. 2d). Pyrite first appeared at the end of the evolution of the carbonatite, in mixed carbonatite and kimberlite-like silicocarbonatite. It is also present in the polygenic breccia as a hydrothermal phase. Similarly, ilmenite, which is relatively reduced compared to magnetite, crystallized throughout most of the evolution of undersaturated silicate magmas and silicocarbonatite, with some magnetite in melteigites and granites. Ilmenite and magnetite are absent in carbonatites, ilmenite re-appears in the kimberlite-like silicocarbonatite, and magnetite replaces it in the polygenic breccia. These results suggest that each magmatic–hydrothermal injection was initially relatively reduced and gradually evolved toward slightly more oxidized compositions before it was cut by a subsequent injection.

Acidic fluids are not compatible with carbonates and carbonatite-hosted magmatic fluids are bound to be neutral to alkaline and contain OH^-, HCO_3^- and $H_2CO_3^0$. In contrast, fluids exsolved from silicate magmas are typically neutral to acidic, especially after vapor–brine unmixing (Webster and Mandeville, 2007) and as acids dissociate upon cooling (Hedenquist and Taran, 2013). At Montviel, mantellic magmatic fluids exsolved from alkaline silicate melts, mixed with crustal fluids and metasomatized the crystallizing silicate rocks, and mantellic magmatic fluids exsolved from silicocarbonatite and carbonatite magmas, mixed with crustal fluids and metasomatized the solidifying carbonatites. Although it appears that silicate and carbonatite magmas originated from distinct mantle pulses, some fluids from the first pulse, especially acidic brines which are denser and tend to pond at depth (Blundy et al., 2015), might have interacted with carbonatites from the second pulse. Consider the very simple exothermic reaction below:

$$2HCl + CaCO_3 \rightarrow H_2O + CO_2 + CaCl_2 \quad \text{(reaction 4)}$$

Hydrochloric acidic fluids in contact with carbonatites would have liberated an important quantity of H_2O and CO_2 (and heat). At low

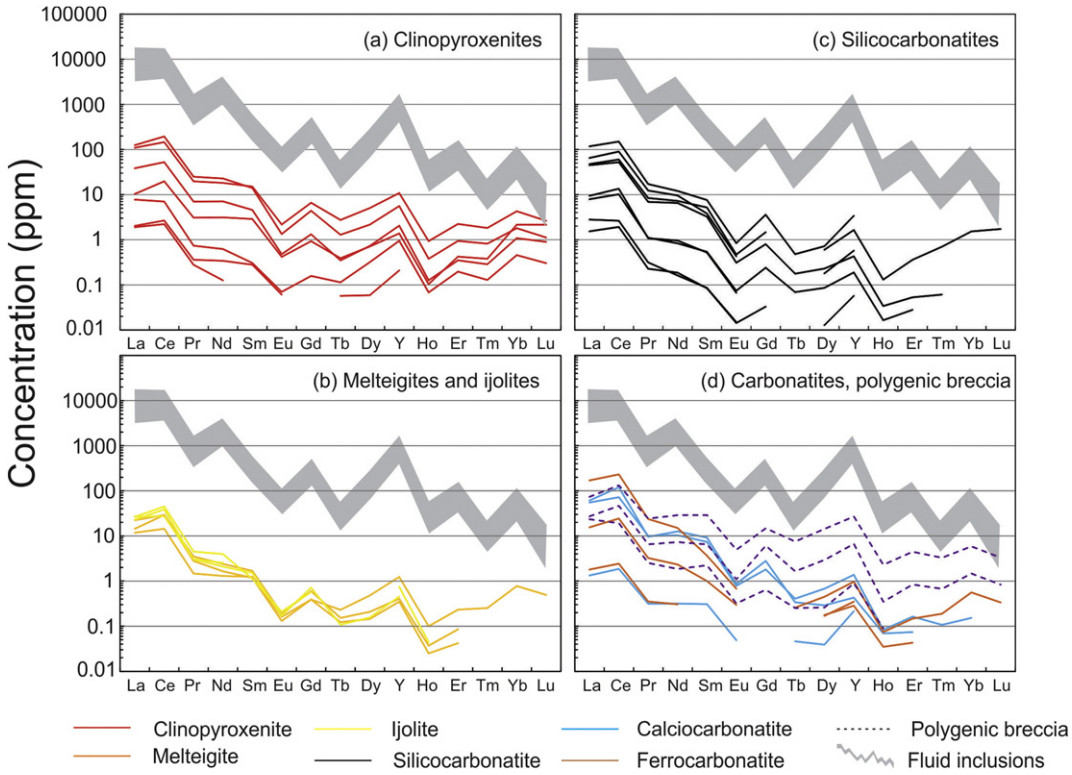

Fig. 13. REE concentration of the fluid in equilibrium with biotite from the different lithologies at Montviel. Calculations are based on mica/fluid partition coefficients in basanite (Adam et al., 2014). The REE concentrations from fluid inclusions are from the Kalkfeld carbonatite complex (Bühn and Rankin, 1999) and the Okorusu carbonatite complex (Bühn et al., 2002), Namibia.

pressures and temperatures, i.e. where these fluids are most acidic, degassing would have increased the pressure possibly to that exceeding the confining pressure, triggering an explosion. We speculate that the injection of acidic fluids with the dyke of kimberlitic silicocarbonatite reacted with carbonatites (reaction 4) which caused the explosion and generated the polygenic breccia.

12. Conclusions

The present paper demonstrates that volatile-saturated alkaline magmas at Montviel evolved by a combination of fractional crystallization, fluid mixing and metasomatism through 4 distinct mantle injections. Each injection had its own mantellic magmatic fluids which mixed with crustal fluids and metasomatized the crystallizing magmas before subsequent fluid-saturated magmas were injected.

At Montviel during the Paleoproterozoic, at 1.894 Ga (David et al., 2006), during a transitional phase between subduction, collision and post-collision relaxation, a first injection of volatile-saturated olivine clinopyroxenite magmas from the mantle evolved to silica-undersaturated melteigites, ijolites and melanosyenites on the one hand, and to silica-saturated syenites and granites on the other hand.

A second mantle pulse resulted in the injection of silicocarbonatites and calciocarbonatites which evolved to REE-bearing ferrocarbonatites also by fractional crystallization, mantle and crustal fluid mixing and metasomatic recrystallization of calcite and dolomite to ferroan dolomite, ankerite and siderite.

A third mantle pulse resulted in inter-mixed dykes, lenses and pods of mineralized silicocarbonatites, calciocarbonatites and ferrocarbonatites and a fourth mantle pulse resulted in the injection of a dyke of volatile-saturated kimberlitic silicocarbonatite. The source of the metasomatic fluids shifted from the mantle to the crust and a catastrophic explosion resulted in the formation of the polygenic breccia. This explosion, which marked the extinction of the system, may have resulted from the interaction of acidic brines from silicate magmas with carbonatites, remobilized the LREE and preferentially enriched the HREE.

At Montviel, it is likely that the carbonatites were not generated directly from partial melting of a pre-metasomatized and carbonated mantle source but instead appear to have resulted from the evolution of clinopyroxenites to silicocarbonatites and carbonatites. At some point during this evolution, carbonatites were separated from silicate magmas so immiscibility cannot be ruled out.

Supplementary data to this article can be found online at http://dx.doi.org/10.1016/j.oregeorev.2015.09.022.

Acknowledgments

This research was funded by NSERC Grant 42576 to M.J. and NSERC Grant 114105 to R.S. We acknowledge the financial, technical and scientific support of Ressource Geomega Inc., S. Britt, A. Cayer and M. Pelletier. This study was also made possible by a FRQNT postdoctoral fellowship to ON. We thank V. Horoi for help with the GIS, L. Shi for help with the electron microprobe, M. Preda and S. Steinhauer for help with the XRD and A. Poirier for help with the TIMS and the LAICPMS. We also thank S. Decrée and an anonymous reviewer for constructive review.

References

Adam, J., Locmelis, M., Afonso, J.C., Rushmer, T., Fiorentini, M.L., 2014. The capacity of hydrous fluids to transport and fractionate incompatible elements and metals within the earth's mantle. Geochem. Geophys. Geosyst. 15, 2241–2253.

Bastrakov, E.N., Skirrow, R.G., Davidson, G.J., 2007. Fluid evolution and origins of iron oxide Cu–Au prospects in the Olympic dam district, gawler craton, South Australia. Econ. Geol. 102, 1415–1440.

Bebout, G.E., 2013. Metasomatism in subduction zones of subducted oceanic slabs, mantle wedges, and the slab-mantle interface. In: Harlov, D.E., Austrheim, H. (Eds.), Metasomatism and the Chemical Transformation of Rock; the Role of Fluids in Terrestrial and Extraterrestrial Processes. Springer, Berlin, Germany, pp. 289–349.

Bell, K., 1998. Radiogenic isotope constraints on relationships between carbonatites and associated silicate rocks; a brief review. J. Petrol. 39, 1987–1996.

Bell, K., Blenkinsop, J., 1989. Neodymium and strontium isotope geochemistry of carbonatites. In: Bell, K. (Ed.), Carbonatites; Genesis and Evolution. Unwin Hyman, London, United Kingdom, pp. 278–300.
Bell, K., Blenkinsop, J., Kwon, S.T., Tilton, G.R., Sage, R.P., 1987. Age and radiogenic isotopic systematics of the Borden carbonatite complex, Ontario, Canada. Can. J. Earth Sci. 24, 24–30.
Best, M.G., Christiansen, E.H., 2001. Igneous Petrology. Blackwell Science.
Black, B.A., Hauri, E.H., Elkins-Tanton, L.T., Brown, S.M., 2014. Sulfur isotopic evidence for sources of volatiles in Siberian traps magmas. Earth Planet. Sci. Lett. 394, 58–69.
Blundy, J., Mavrogenes, J., Tattitch, B., Sparks, S., Gilmer, A., 2015. Generation of porphyry copper deposits by gas–brine reaction in volcanic arcs. Nat. Geosci. 8, 235–240.
Bowen, N.L., 1928. The evolution of the igneous rocks. Princeton University Press.
Brooker, R.A., Kjarsgaard, B.A., 2011. Silicate–carbonate liquid immiscibility and phase relations in the system SiO_2–Na_2O–Al_2O_3–CaO–CO_2 at 0. 1–2. 5 GPa with applications to carbonatite genesis. J. Petrol. 52, 1281–1305.
Bühn, B., Rankin, A.H., 1999. Composition of natural, volatile-rich Na–Ca–REE–Sr carbonatitic fluids trapped in fluid inclusions. Geochim. Cosmochim. Acta 63, 3781–3797.
Bühn, B., Rankin, A.H., Schneider, J., Dulski, P., 2002. The nature of orthomagmatic, carbonatitic fluids precipitating REE, Sr-rich fluorite: fluid-inclusion evidence from the Okorusu fluorite deposit, Namibia. Chem. Geol. 186, 75–98.
Chakhmouradian, A.R., Zaitsev, A.N., 2012. Rare earth mineralization in igneous rocks; sources and processes. Elements 8, 347–353.
Condie, K., Pisarevsky, S.A., Korenaga, J., Gardoll, S., 2015. Is the rate of supercontinent assembly changing with time? Precambrian Res. 259, 278–289.
Corriveau, L., 2007. Iron oxide copper–gold deposits; a Canadian perspective. Special publication — Geological Association of Canada. Miner. Deposits Div. 5, 307–328.
David, J., Dion, C., Goutier, J., Roy, P., Bandyayera, D., Legault, M., Rhéaume, P., 2006. Datations U–Pb effectuées dans la Sous-province de l'Abitibi à la suite des travaux de 2004–2005. MRNF Québec, Québec, RP 2006-04.
deMoor, J.M., Fischer, T.P., King, P.L., Botcharnikov, R.E., Hervig, R.L., Hilton, D.R., Barry, P.H., Mangasini, F., Ramirez, C., 2013. Volatile-rich silicate melts from oldoinyo lengai volcano (Tanzania): implications for carbonatite genesis and eruptive behavior. Earth Planet. Sci. Lett. 361, 379–390.
Desharnais, G., Duplessis, C., 2011. Montviel Core Zone REE Mineral Resource Estimate Technical Report. Private Report (74 pp.).
Drüppel, K., Hoefs, J., Okrusch, M., 2005. Fenitizing processes induced by ferrocarbonatite magmatism at Swartbooisdrif, NW Namibia. J. Petrol. 46, 377–406.
Dupuy, C., Mevel, C., Bodinier, J.-L., Savoyant, L., 1991. Zabargad peridotite; evidence for multistage metasomatism during Red Sea rifting. Geology 19, 722–725.
Elsdon, R., 1982. Autometasomatic alteration of Gabbro, KapEdvard Holm intrusive complex, east Greenland. Mineral. Mag. 45, 219–225.
Erić, S., Logar, M., Milovanović, D., Babič, D., Adnađević, B., 2009. Ti-in-biotite geothermometry in non-graphitic, peraluminous metapelites from Crnivrh and Resavskihumovi (central Serbia). Geol. Carpath. (Bratislava) 60, 3–14.
Fall, A., Bodnar, R.J., Szabó, C., Pál-Molnár, E., 2007. Fluid evolution in the nepheline syenites of the ditrău alkaline massif, Transylvania, Romania. Lithos 95 (3–4), 331–345.
Gittins, J., 1989. The origin and evolution of carbonatite magmas. In: Bell, K. (Ed.), Carbonatites Genesis and Evolution. UnwinHyman Ltd, pp. 580–599.
Goutier, J., 2006. Géologie de la région du Lac au goéland (32F15), Quebec, RG 2005-05 (39 pp.).
Hamilton, D.L., Burnham, C.W., Osborn, E.F., 1964. The solubility of water and effects of oxygen fugacity and water content on crystallization in mafic magmas. J. Petrol. 5 (Part 1), 21–39.
Hedenquist, J.W., Lowenstern, J.B., 1994. The role of magmas in the formation of hydrothermal ore deposits. Nature 370, 519–527.
Hedenquist, J.W., Taran, Y.A., 2013. Modeling the formation of advanced argillic lithocaps: volcanic vapor condensation above porphyry intrusions. Econ. Geol. 108, 1523–1540.
Henry, D.J., Guidotti, C.V., Thomson, J.A., 2005. The Ti-saturation surface for low-to-medium pressure metapelitic biotites: implications for geothermometry and Ti-substitution mechanisms. Am. Mineral. 90, 316–328.
Jacobsen, S.B., 1988. Isotopic constraints on crustal growth and recycling. Earth Planet. Sci. Lett. 90, 315–329.
Jébrak, M., 1997. Hydrothermal breccias in vein-type ore deposits; a review of mechanisms, morphology and size distribution. Ore Geol. Rev. 12, 111–134.
Kerrich, R., Cassidy, K.F., 1994. Temporal relationships of lode gold mineralization to accretion, magmatism, metamorphism and deformation; archean to present; a review. Ore Geol. Rev. 9, 263–310.
Kjarsgaard, B.A., Hamilton, D.L., 1989. The genesis of carbonatites by immiscibility. In: Bell, K. (Ed.), Carbonatites Genesis and Evolution. Unwin Hyman Ltd., pp. 388–403.
Landoll, J.D., Foland, K.A., 1996. The formation of quartz syenite by crustal contamination at the Mount Shefford and other Monteregian Hills complexes. Can. Mineral. 34, 301–324.
Le Bas, M., 1977. Carbonatite Nepheline Volcanism. John Wiley & Sons, New York.
Lee, W.-J., Wyllie, P.J., 1998. Processes of crustal carbonatite formation by liquid immiscibility and differentiation, elucidated by model systems. J. Petrol. 39, 2005–2013.
Lindgren, W., 1933. Mineral deposits. 4th ed. (930 pp.).
Mueller, W.U., Daigneault, R., Mortensen, J.K., Chown, E.H., 1996. Archean terrane docking; upper crust collision tectonics, Abitibi Greenstone Belt, Quebec, Canada. Tectonophysics 265, 127–150.
Nadeau, O., Cayer, A., Pelletier, M., Séguin, D., Stevenson, R., Jébrak, M., 2013. Pétro-Métallogenèse du Système Alcalin Carbonatitique (REE–Nb) de Montviel, Abitibi. Québec Mines, MRNF, Québec, Canada.
Nadeau, O., Cayer, A., Pelletier, M., Stevenson, R., Jébrak, M., 2015. The paleoproterozoic Montviel carbonatite-hosted REE–Nb deposit, Abitibi, Canada: geology, mineralogy, geochemistry and genesis. Ore Geol. Rev. 67, 314–335.
Neuhoff, P.S., Hovis, G.L., Balassone, G., Stebbins, J.F., 2004. Thermodynamic properties of analcime solid solutions. Am. J. Sci. 304, 21–66.
O'Reilly, S.Y., Griffin, W.L., 2013. Mantle metasomatism. In: Harlov, D.E., Austrheim, H. (Eds.), Metasomatism and the Chemical Transformation of Rock. Springer, Oslo, Norway, pp. 471–533.
Patiño-Douce, A.E.P., 1993. Titanium substitution in biotite: an empirical model with applications to thermometry, O_2 and H_2O barometries, and consequences for biotite stability. Chem. Geol. 108, 133–162.
Pirajno, F., 2013. Effects of metasomatism on mineral systems and their host rocks; alkali metasomatism, skarns, greisens, tourmalinites, rodingites, black-wall alteration and listvenites. In: Harlov, D.E., Austrheim, H. (Eds.), Metasomatism and the Chemical Transformation of Rock; the Role of Fluids in Terrestrial and Extraterrestrial Processes. Springer, Berlin, Germany, pp. 203–251.
Pirajno, F., 2015. Intracontinental anorogenic alkaline magmatism and carbonatites, associated mineral systems and the mantle plume connection. Gondwana Res. 27, 1181–1216.
Plail, M., Edmonds, M., Humphreys, M.C.S., Barclay, J., Herd, R.A., 2014. Geochemical evidence for relict degassing pathways preserved in andesite. Earth Planet. Sci. Lett. 386, 21–33.
Ramberg, H., 1952. The origin of metamorphic and metasomatic rocks (317 pp.).
Richards, J.P., 2014. Discussion of: the link between reduced porphyry copper deposits and oxidized magmas. Geochim. Cosmochim. Acta 126, 643–645.
Roulleau, E., Stevenson, R., 2013. Geochemical and isotopic (Nd–Sr–Hf–Pb) evidence for a lithospheric mantle source in the formation of the alkaline monteregian province (Quebec). Can. J. Earth Sci. 50, 650–666.
Sage, R.P., 1988. Geology of carbonatite–alkalic rock complexes in Ontario; Cargill Township Carbonatite Complex, District of Cochrane. Ontario Geological Survey, Toronto, ON, Canada.
Seedorff, E., Dilles, J.H., Proffett Jr., J.M., Einaudi, M.T., Zurcher, L., Stavast, W.J.A., Johnson, D.A., Barton, M.D., 2005. Porphyry deposits; characteristics and origin of hypogene features. In: Hedenquist, J.W.T., John, F.H., Goldfarb, R.J., Richards, J.P. (Eds.), Economic Geology; one Hundredth Anniversary Volume. Society of Economic Geologists, United States, pp. 1905–2005.
Sillitoe, R.H., 1973. The tops and bottoms of porphyry copper deposits. Econ. Geol. 68, 799–815.
Sillitoe, R.H., 2010. Porphyry copper systems. Econ. Geol. Bull. Soc. Econ. Geol. 105, 3–41.
Sirbescu, M., Jenkins, D.M., 1999. Experiments on the stability of cancrinite in the system Na_2O–CaO–Al_2O_3–SiO_2–CO_2–H_2O. Am. Mineral. 84, 1850–1860.
Smith, M.P., Campbell, L.S., Kynicky, J., 2015. A review of the genesis of the world class bayan Obo Fe–REE–Nb deposits, Inner Mongolia, China: multistage processes and outstanding questions. Ore Geol. Rev. 64, 459–476.
Sun, S.S., McDonough, W.F., 1989. Chemical and isotopic systematics of oceanic basalts; implications for mantle composition and processes. In: Saunders, A.D. (Ed.), Magmatism in the Ocean Basins. Geological Society of London, London, United Kingdom, pp. 313–345.
Tomisaka, T., Eugster, H.P., 1968. Synthesis of the sodalite group and subsolidus equilibria in the sodalite–noselite system. Mineral. J. 5, 249–275.
Touret, J.L.R., Nijland, T.G., 2013. Prograde, peak and retrograde metamorphic fluids and associated metasomatism in upper amphibolite to granulite facies transition zones. In: Harlov, D.E., Austrheim, H. (Eds.), Metasomatism and the Chemical Transformation of Rock; the Role of Fluids in Terrestrial and Extraterrestrial Processes. Springer, Berlin, Germany, pp. 415–469.
Tuttle, O.F., Smith, J.V., 1958. Nepheline–kalsilite system II. Phase relations. Am. J. Sci. 256, 571–589.
Washington, H.S., 1901. The foyaite–ijolite series of magnet cove [Arkansas]; a chemical study in differentiation. J. Geol. 607-622.
Webster, J.D., Mandeville, C.W., 2007. Fluid immiscibility in volcanic environments. Rev. Mineral. Geochem. 65, 313–362.
Woolley, A.R., Kempe, D.R.C., 1989. Carbonatites; nomenclature, average chemical compositions, and element distribution. In: Bell, K. (Ed.), Carbonatites; Genesis and Evolution. Unwin Hyman, London, United Kingdom, pp. 1–14.
Wyllie, P.J., Jones, A.P., Deng, J., 1989. Origin of carbonatites: evidence from phase equilibrium studies. In: Bell, K. (Ed.), Carbonatites Genesis and Evolution. Unwin Hyman Ltd, pp. 500–540.